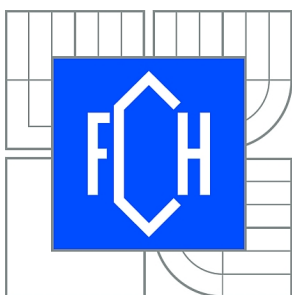




VYSOKÉ UČENÍ TECHNICKÉ V BRNĚ

BRNO UNIVERSITY OF TECHNOLOGY



FAKULTA CHEMICKÁ

ÚSTAV FYZIKÁLNÍ A SPOTŘEBNÍ CHEMIE

FACULTY OF CHEMISTRY

INSTITUTE OF PHYSICAL AND APPLIED CHEMISTRY

SOL-GEL PROCESS USING REVERSE MICELLES

SOL-GEL PROCES S REVERZNÍMI MICELAMI

DIPLOMOVÁ PRÁCE

MASTER'S THESIS

AUTOR PRÁCE

AUTHOR

Ing. MAGDALENA LUKEŠOVÁ

VEDOUCÍ PRÁCE

SUPERVISOR

doc. Ing. MICHAL VESELÝ, CSc.

BRNO 2011



Vysoké učení technické v Brně
Fakulta chemická
Purkyňova 464/118, 61200 Brno 12

Zadání diplomové práce

Číslo diplomové práce:	FCH-DIP0497/2010	Akademický rok: 2010/2011
Ústav:	Ústav fyzikální a spotřební chemie	
Student(ka):	Ing. Magdalena Lukešová	
Studijní program:	Spotřební chemie (N2806)	
Studijní obor:	Spotřební chemie (2806T002)	
Vedoucí práce	doc. Ing. Michal Veselý, CSc.	
Konzultanti:		

Název diplomové práce:

Sol-gel proces s reverzními micelami

Zadání diplomové práce:

1. Literární rešerše na téma příprava vrstev oxidu titaničitého sol-gel procesem s využitím reverzních micel.
2. Příprava vybrané kompozice solu a její aplikace tiskem.
3. Ověření fotokatalytické účinnosti připravených vrstev.

Termín odevzdání diplomové práce: 13.5.2011

Diplomová práce se odevzdává ve třech exemplářích na sekretariát ústavu a v elektronické formě vedoucímu diplomové práce. Toto zadání je přílohou diplomové práce.

Ing. Magdalena Lukešová
Student(ka)

doc. Ing. Michal Veselý, CSc.
Vedoucí práce

prof. Ing. Miloslav Pekař, CSc.
Ředitel ústavu

V Brně, dne 15.1.2011

prof. Ing. Jaromír Havlica, DrSc.
Děkan fakulty

ABSTRAKT

Práce popisuje přípravu tenkých transparentních vrstev oxidu titaničitého metodou sol-gel procesu s reverzními micelami, které jsou jedinečným uskupením zajišťujícím uniformní velikost připravených částic. Neionogenní tenzid byl použit jako templát. Pomocí materiálového tisku, tedy specializovanou formou inkoustového tisku, byly připraveny tenké filmy TiO_2 nanesením 1–4 vrstev. Po kalcinaci byly připravené vrstvy oxidu titaničitého charakterizované šířkou zakázaného pásu. Struktura vrstev byla popsána optickou mikroskopií a SEM. Fotokatalytická aktivita byla ověřena oxidační reakcí 2,6-dichlorindofenolu a rozkladem kyseliny stearové, která byla přímo natištěna na vrstvy oxidu titaničitého. Fotoindukovaná změna hydrofility byla studována pomocí měření kontaktního úhlu smáčení vody. Fotokatalytická účinnost připravených filmů rostla s počtem vrstev oxidu titaničitého.

ABSTRACT

This study describes preparation of transparent thin films of TiO_2 by sol-gel process with reverse micelles, which represent a unique system for production of uniform particles. A non-ionic surfactant was used as a templating agent. Material printing as a specialized inkjet printing technique was used to prepare titania thin films of 1–4 layers. After calcination the prepared films of titanium dioxide were characterised by band gap energy. The structure of the films was described by optical microscopy and SEM. Photocatalytic activity was verified by oxidation reaction of 2,6-dichloroinfophenol and by degradation of stearic acid directly printed on the active layers. Photo-induced hydrophilicity was characterised by contact angle measurement of water wettability. Photocatalytic efficiency of prepared films increased with increasing number of titania layers.

KLÍČOVÁ SLOVA

oxid titaničitý, sol-gel, reverzní micely, materiálový tisk, fotokatalýza, foto-indukovaná hydrofilita

KEY WORDS

titanium dioxide, sol-gel, reverse micelles, material printing, photocatalysis, photo-induced hydrophilicity

LUKEŠOVÁ, M. *Sol-gel proces s reverzními micelami*. Brno: Vysoké učení technické v Brně, Fakulta chemická, 2011. 68 s. Vedoucí diplomové práce
doc. Ing. Michal Veselý, CSc.

DECLARATION

I declare that the diploma thesis has been worked out by myself and that all the quotations from the used literary sources are accurate and complete. The content of the diploma thesis is the property of the Faculty of Chemistry of Brno University of Technology and all commercial uses are allowed only if approved by both the supervisor and the dean of the Faculty of Chemistry, BUT.

.....
student's signature

Sincere acknowledgement belongs to doc. Ing. Michal Veselý, CSc. and the whole team from the photochemical laboratory.

*I hear and I forget.
I see and I remember.
I do and I understand.*

Confucius

CONTENTS

1	INTRODUCTION	8
2	THEORETICAL PART	9
2.1	Heterogeneous photocatalysis	9
2.2	Titanium dioxide	9
2.3	Titanium dioxide photocatalysis	11
2.3.1	Oxidation-reduction reactions	11
2.3.2	Characteristics of photocatalytic processes.....	12
2.3.2.1	<i>Environmental semiconductor photocatalysis</i>	<i>13</i>
2.4	Kinetics of heterogeneous photocatalytic reactions	14
2.4.1	Langmuir-Hinshelwood kinetics	14
2.5	Preparation of TiO ₂	16
2.5.1	Sol-gel method	16
2.5.2	Sol-gel method with reverse micelles	17
2.5.3	Hydrothermal/solvothermal method	18
2.6	Deposition techniques	18
2.6.1	Dip coating	19
2.6.2	Spin coating.....	20
2.6.3	Inkjet printing.....	20
2.6.4	Material printing.....	22
2.6.4.1	<i>Material printing applications</i>	<i>22</i>
2.6.4.2	<i>Specialized printing device</i>	<i>23</i>
2.6.5	Chemical vapour deposition.....	23
2.7	Aspects effecting the TiO ₂ film structure.....	23
2.7.1	Effect of calcination temperature and calcination time.....	24
2.7.2	Substrate and coating solution	25
2.7.3	Role of the template molecular structure	25
2.7.4	Number of coating cycles.....	26
2.8	Pre-treatment of soda-lime glass support	26
2.9	Chemical reactors	26
2.10	Characterization of TiO ₂ films	27
2.10.1	Photocatalytic activity of TiO ₂ films.....	27
2.10.1.1	<i>Photocatalytic oxidation of 2,6-dichloroindophenole.....</i>	<i>27</i>
2.10.1.2	<i>Photocatalytic degradation of stearic acid.....</i>	<i>28</i>
2.10.2	Contact angle measurement	28
2.10.2.1	<i>Photo-induced hydrophilicity.....</i>	<i>30</i>
2.10.3	Band gap determination	30
2.11	Instruments for TiO ₂ films characterization.....	32
2.11.1	UV/VIS spectrophotometry	32
2.11.2	Optical microscopy/Digital microphotography.....	32

2.11.3	FT-IR spectrometry	33
2.11.4	Scanning electron microscopy	35
3	EXPERIMENTAL	36
3.1	Chemicals, devices and software.....	36
3.1.1	Chemicals.....	36
3.1.2	Devices.....	36
3.1.3	Software	36
3.2	Titanium dioxide film deposition.....	37
3.2.1	Substrate pretreatment.....	37
3.2.2	Sol synthesis.....	37
3.2.3	Deposition of layers	38
3.3	Description of layers	40
3.3.1	Optical microscopy/Digital microphotography.....	40
3.3.2	Scanning electron microscopy	40
3.3.3	Photoinduced hydrophilicity	40
3.4	Photocatalytic experiments.....	41
3.4.1	Photocatalytic degradation of 2,6-dichloroindophenol.....	41
3.4.2	Photocatalytic degradation of stearic acid.....	43
	3.4.2.1 Stearic acid deposition.....	43
	3.4.2.2 FT-IR spectrometry.....	44
	3.4.2.3 Contact angle measurement.....	44
3.5	Band gap determination.....	44
4	RESULTS AND DISSCUSSION	45
4.1	Dynamic viscosity determination.....	45
4.2	Optical microscopy.....	45
4.3	Scanning electron microscopy.....	47
4.4	Band gap determination.....	48
4.5	Photoinduced hydrophilicity	51
4.6	Photocatalytic activity of 2,6-dichloroindophenol	53
4.6.1	Calibration curve method.....	53
4.6.2	Photochemical degradation of 2,6-dichloroindophenol	55
4.7	Photocatalytic activity of stearic acid.....	58
4.7.1	Photocatalytic degradation of stearic acid.....	58
4.7.2	Contact angle measurement	60
5	CONCLUSION	62
6	REFERENCES.....	63
7	LIST OF ABBREVIATIONS.....	68

1 INTRODUCTION

Environmental pollution is one of the serious problems all around the world. Photocatalytic technology that is a widely studied topic could be effective in the environmental cleanup⁸. Titanium dioxide belongs to the group of popular and promising materials for photocatalytic applications, such as photocatalytic, photovoltaic, photoinduced superhydrophilical applications etc. According to the requirement of the application, titanium dioxide is needed to be modified. It is therefore very important to study the evolution of different physical and chemical properties of TiO₂, prepared by a suitable technique which is effective for controlled modification¹.

Among the various techniques to prepare TiO₂ in immobilized form the most widely used one is the sol-gel method because of its ability to obtain films with tailored properties. TiO₂ film is prepared from alkoxide solution, where metal alkoxide precursor is hydrolyzed under controlled conditions to form an extensive three dimensional network. Sol-gel process with reverse micelles represents a unique system for production of uniform particles.

A possibility was found to improve the properties of titania thin films obtained by this way by means of suitable modification of the precursor with different agents. Added acetylacetone leads to slowing down of the sol-gel process and thus stabilizes the sol. Furthermore, modification by polyols such as polyethyleneglycol has a strong effect on gelation time, particle morphology, porosity, etc.

High surface area mesostructured TiO₂ is used in photocatalysis for purification of water or air, for decomposing germs, viruses and dirt. The absorption characteristics allow titanium dioxide to absorb photons of UV light, producing reactive electron-hole pairs that can react with surrounding materials. The durability and stability of TiO₂ during such reactions make it an ideal material for any application where the material is to be used continuously without frequent replacement⁸.

Titania semiconductor in a form of powder or a film can be used to study photocatalytic properties. The major problem of the powder form of semiconductor in the practical applications is the cost of the separation step necessary after the purification. Therefore, an immobilized system is preferred for an efficient reactor suitable for industrial sizes, especially since the efficiency of the immobilized system can be comparable to that of the suspended system. An important issue is also an immobilization technique that would provide even thin films of desired properties. Material printing, as a special form of inkjet printing, should be mentioned as a promising deposition technique preferred to other deposition techniques used for thin titania films preparation.

The aim of this thesis was to summarize an actual aspect of the solved topic. This study also describes a method for preparing titanium dioxide thin films via sol-gel process with reverse micelles. In the next step photoinduced superhydrophilicity and photocatalysis were studied on TiO₂ coated soda-lime glass plates.

2 THEORETICAL PART

2.1 Heterogeneous photocatalysis

Heterogeneous photocatalysis (HP) involves photoreactions which occur at the surface of a catalyst. Basic principles of HP are as follows.

A semiconductor (SC) is characterized by an electronic band structure in which the highest occupied energy band, called valence band (VB), and the lowest empty band, called conduction band (CB), are separated by a band gap. When a photon of energy higher or equal to the band gap energy is absorbed by a SC particle, an electron from the VB is promoted to the CB with simultaneous generation of a hole (h^+) in the VB (Figure 1). The e_{CB}^- and h_{VB}^+ can recombine on the surface or in the bulk of the particle in few nanoseconds (energy is dissipated as heat) or can be trapped in surface states where they can react with donor or acceptor species adsorbed at the surface of the particle. Thereby, subsequently redox reactions can be initiated.

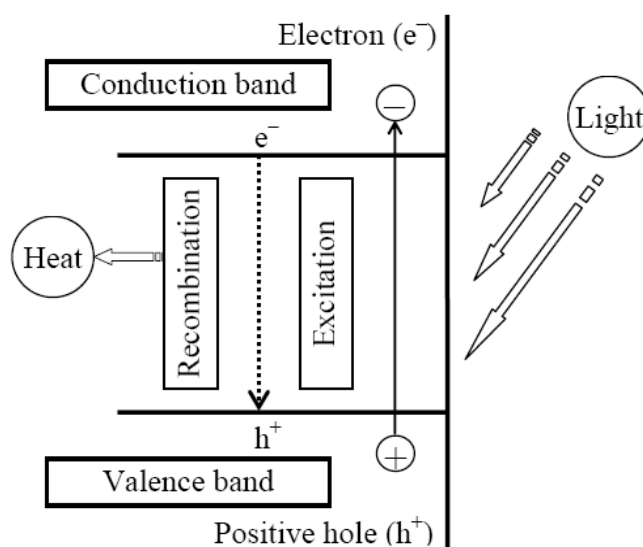


Figure 1 Simplified diagram of the heterogeneous photocatalytic processes on an illuminated semiconductor particle

Various factors can affect the photocatalytic reaction rate. For example, the pH of the solution determines the surface charge on the SC. Photocatalytic reactions originate in the interface, so adsorption processes seem to have a particular importance. The kinetics depends on the substrate concentration and also access of light, which promotes a faster electron-hole recombination. High temperatures generally lead to higher rates because they provoke a more frequent collision between the substrate and the SC. The presence of metal ions or inorganic anions in the solution is also of great importance².

2.2 Titanium dioxide

Titanium dioxide, or titanium(IV) oxide, is a naturally existing semiconductor in three crystallographic forms – anatase, brookite and rutile (Figure 2), all with 6-coordinate titanium:

Rutile form – the most common form in tetragonal symmetry ($a = 4.594 \text{ \AA}$, $c = 2.958 \text{ \AA}$), exists both in nature and produced commercially. It is a high pressure and temperature mineral found in igneous rocks³.

Anatase form – tetragonal ($a = 3.793 \text{ \AA}$, $c = 9.51 \text{ \AA}$) crystal, which looks like stretched out octahedrons. It is stable at low temperature; at about $915 \text{ }^\circ\text{C}$ reverts to the rutile structure.

Brookite – titanium dioxide in an orthorhombic symmetry ($a = 5.456 \text{ \AA}$, $b = 9.182 \text{ \AA}$, $c = 5.143 \text{ \AA}$). It is also stable at low temperatures and reverts to rutile at about $750 \text{ }^\circ\text{C}$.

Transition between individual crystal forms of titanium dioxide occurs as follows:

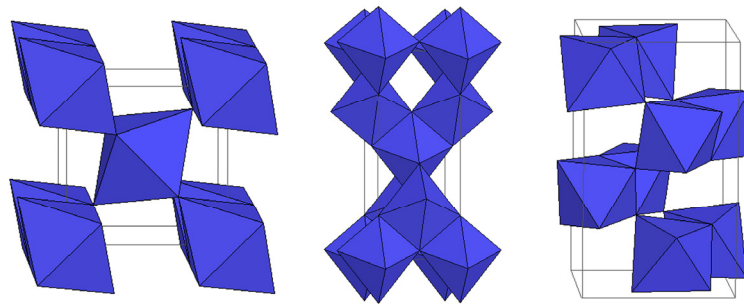
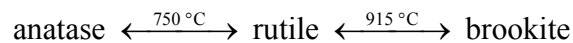


Figure 2 The crystal structure of rutile (left), anatase (middle) and brookite (right)

The material properties of TiO_2 nanoparticles are a function of the crystal structure, nanoparticle size and morphology and are strongly dependant on the method of synthesis. As a bulk material, rutile is the stable phase; however, solution-phase preparation methods for TiO_2 generally favour the anatase structure⁴.

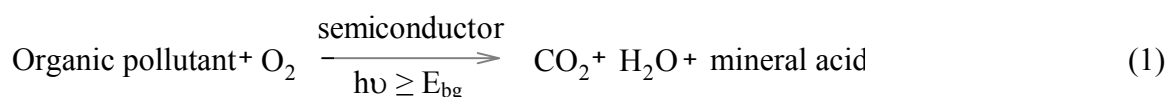
It is generally assumed that anatase allows a higher photocatalytic activity than rutile and brookite⁵. One of the reasons why the anatase type titanium dioxide is more photoactive than the rutile type is the differences in their so called energy band structures. The band gap energy for a semiconductor indicates the minimum energy of light to produce conduction band electrons and valence band holes. Both the holes and the hydroxyl radicals are very powerful oxidants, which can be used to oxidize most organic materials.

For anatase-type titanium dioxide the band gap energy is 3.2 eV , which corresponds to UV light (388 nm), while the band gap energy for rutile type is 3.0 eV , corresponding to violet light (413 nm). The valence band energies for anatase and rutile are both similar; the VB holes (and hydroxyl radicals $\cdot\text{OH}$) have great oxidizing power. The difference between anatase and rutile is in a conduction band. The conduction band for anatase is higher than for rutile in the energy diagram meaning that it has higher reducing power; it can drive very important reaction involving reduction of molecular oxygen O_2 to superoxide $\text{O}_2^{\cdot-}$. This issue is further discussed in the chapter 2.3.1.

2.3 Titanium dioxide photocatalysis

2.3.1 Oxidation-reduction reactions

The reaction starts with the exposure of titanium dioxide to light. As mentioned in Chapter 2.1, two types of carriers are generated – electrons e^- and holes h^+ . On semiconductors such as TiO_2 these two survive for longer periods of time than e.g. in electrically conductive materials. On the surface of the catalyst, there is approximately a single layer of tightly adhering adsorbed water molecules. When these adsorbed water molecules are oxidized by holes, hydroxyl radicals $\cdot OH$ are formed (see Figure 3). The hydroxyl radicals can then react with organic compounds, producing free radicals, which are unstable molecules with one unpaired electron. When molecular oxygen with unpaired electrons is present, it likes to react with these free radicals, producing organic peroxy radicals. These can then take part in chain reactions, where organic compounds are completely degraded into carbon dioxide and water in a short time. The longer the film is illuminated with UV light, the more organic material can be decomposed (equation (1)), where E_{bg} is the band gap energy of the semiconductor)^{6,7}.



The electrons that are produced in the electron-hole pairs are also put to work. These electrons are used to add electrons (reduce) to oxygen in the air. Oxygen is reduced easier than water to produce superoxide radical anion $O_2^{\cdot -}$. This $O_2^{\cdot -}$ attaches peroxy radicals resulting in unstable product containing now at least four oxygens that can decompose to produce a carbon dioxide molecule. Superoxide acts like a “supercharger” greatly increasing the oxidation process.

In general, organic compounds are more likely to be oxidized than water. Therefore, when the concentration of the organic compound is high, the photogenerated holes will react directly with these compounds (holes are effectively trapped) instead of reacting with water to produce $\cdot OH$, which increases the overall efficiency. Consequently, the rate-determining step is the speed of the transfer of electrons to oxygen.

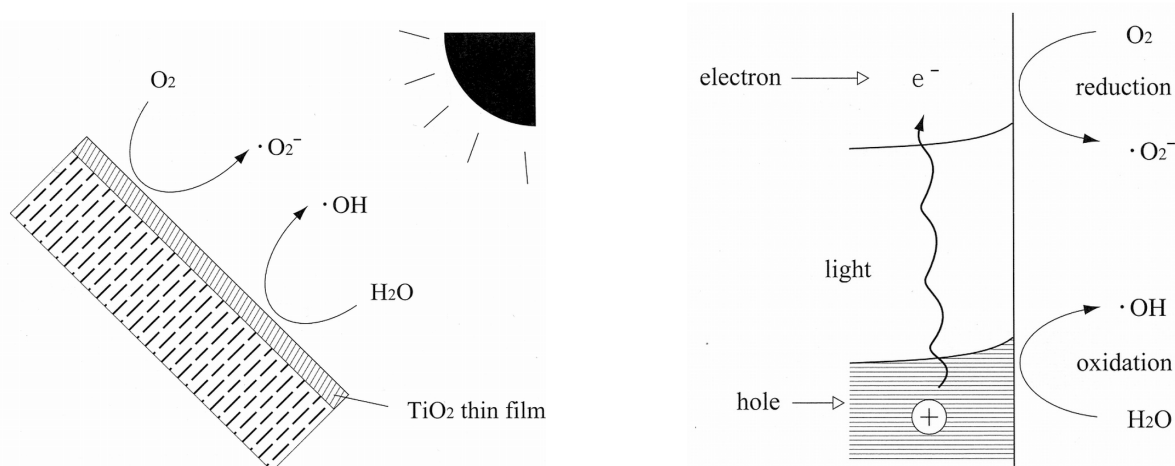


Figure 3 Reaction mechanism of TiO_2 photocatalysis

2.3.2 Characteristics of photocatalytic processes

Titanium dioxide is chemically activated by light energy. For a long time, photoactivity has been considered a problem, as titanium dioxide was used as a pigment. It decomposes organic materials that come in contact with it. This effect gives rise to the phenomenon of paint chalking, where the organic components of the paint break down as a result of photocatalytic action.

On the other hand, titanium dioxide photoactivity plays a positive role – decomposing materials of our choice, e.g. dirt, toxic chemicals, bacteria, etc⁶.

Titanium dioxide is widely used in the area of environmental photocatalysis and for its photoinduced hydrophilicity². The photocatalytic technology is applied to the decomposition of materials that are carried to the surface from surrounding environment. The superhydrophilic effect, on the other hand, is based on a concept of altering the properties of the surface itself by photocatalytic action. While both technologies are applied to the prevention of soiling, their basic mechanisms are quite different from each other (Figure 4). Hydrophilicity and photocatalysis take place simultaneously on the same TiO₂ surface but in varying proportions, depending on the desired application. It can be also concluded that the most appropriate applications for the photocatalytic approach would be those that involve low concentrations of matter that are of serious risks to health or comfort.

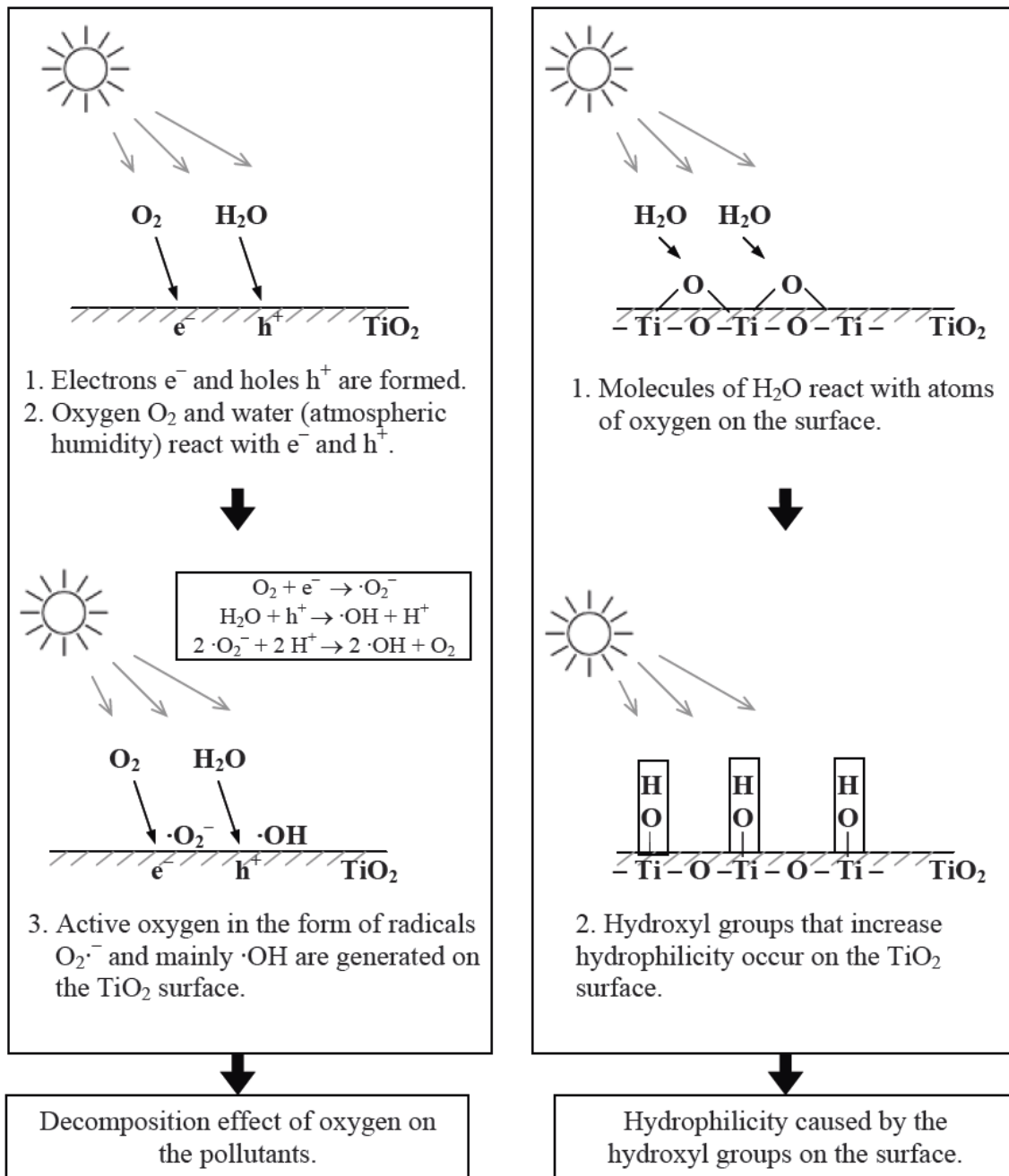


Figure 4 Characteristics of photocatalytic processes

2.3.2.1 Environmental semiconductor photocatalysis

The use of titanium dioxide in photocatalysis is dependent on the absorption characteristics, which allow it to absorb photons of UV light, producing reactive electron-hole pairs that can react with surrounding materials. The durability and stability of TiO₂ during such reactions make it an ideal material for any application where the material is to be used continuously without frequent replacement⁸.

Some of the applications and supporting technology have been reported in the literature, including the development of TiO₂ films, TiO₂-containing paper or tiles with photocatalytic antimicrobial and stain resistant surface were fabricated. Another application in photocatalytic

technology is flow-type photoreactor for water purification. Also self-cleaning TiO₂-coated glass covers for highway tunnel lamps, self-cleaning window glass and building materials or TiO₂-containing self-cleaning paint should be mentioned.

Self-cleaning materials based on photocatalysts are able to clean without toxic chemicals, which is definitely a great advantage. However, these materials cannot do miracles; buildup of dirt can occur if the deposition of contaminants is faster than the speed of their decomposition. Also, if the dirt thickness is too high, no light can reach the titanium dioxide surface, than no reaction occurs⁶.

2.4 Kinetics of heterogeneous photocatalytic reactions

Heterogeneous photocatalytic process is a reaction between a photoinduced charge carriers and an adsorbed reagent on the photocatalyst surface (solid phase), which evokes chemical changes of the reactant (gaseous or liquid phase). The photocatalytic reaction runs in partial sequential steps⁹:

- reagent transport from the liquid (gaseous) phase to the photocatalyst surface
- reagent adsorption on the photocatalyst surface
- chemical reaction on the photocatalyst surface
- product desorption from the photocatalyst surface
- product transport into the liquid (gaseous) phase.

The overall reaction rate depends on the reaction rate of each individual step of the whole process. Reagent transport to the photocatalyst surface is caused by convection and diffusion, in other words, it generally depends on the hydrodynamic and diffusive character of the system (gas or liquid circulation, particle size, diffusion coefficients, etc.). Diffusion of the reagent through the porous structure of the solid photocatalyst depends on the pore size, the particle size, diffusion coefficients and concentration gradients of the reagents.

The transport rate of the reagents is higher than the reaction rate in the reactor; therefore it is not the determining step for the overall reaction rate. The overall reaction rate is mostly dependent on the reagent adsorption and the chemical reaction on the solid photocatalytic surface.

2.4.1 Langmuir-Hinshelwood kinetics

Langmuir-Hinshelwood (LH) kinetics is the most commonly used kinetic expression to explain the kinetics of the heterogeneous catalytic processes¹⁰. In LH models, the surface of the catalyst is modeled as being energetically uniform and it is assumed that there is no energetic interaction between species adsorbed on the surface. Each reactant is assumed to adsorb on a surface site. Following surface reaction between adsorbed reactants to generate surface products, the products desorb from the surface¹¹. Heterogeneous surface catalytic reaction mechanism is based on the reaction between molecular fragments and atoms adsorbed on the catalyst surface. Therefore, these reactions are the second order reactions¹⁴:



The reaction rate is:

$$v = k \cdot \theta_A \cdot \theta_B \quad (3)$$

Using the Langmuir isotherms for A and B, the adsorption runs without dissociation:

$$\theta_A = \frac{K_A \cdot c_A}{1 + K_A \cdot c_A + K_B \cdot c_B} \quad (4)$$

$$\theta_B = \frac{K_B \cdot c_B}{1 + K_A \cdot c_A + K_B \cdot c_B} \quad (5)$$

where θ is a concentration of sites covered with A or B. K_A , K_B are the adsorption constants of the reactants A and B; c_A and c_B are concentrations of A and B.

Applying the expressions (4) a (5) on the expression (3), we obtain the following equation for the reaction rate v :

$$v = \frac{k \cdot K_A \cdot K_B \cdot c_A \cdot c_B}{(1 + K_A \cdot c_A + K_B \cdot c_B)^2} \quad (6)$$

The rate constant k and isothermal parameters K_A and K_B are thermally dependent.

The kinetics of the heterogeneous catalytic reactions can be simply qualified by the reaction rate equation (Langmuir-Hinshelwood equation):

$$v = \frac{k \cdot K \cdot c}{1 + K \cdot c} \quad (\text{per gram of photocatalyst}) \quad (7)$$

For practical application a linearized equation (7) is used. This is obtained using the dependence of reciprocal initiative rate over reciprocal initiative concentration:

$$\frac{1}{v} = \frac{1}{k} + \frac{1}{k \cdot K} \cdot \frac{1}{c} \quad (8)$$

At lower concentrations. reaction is simplified to the first order:

$$v = k \cdot K \cdot c \quad (9)$$

The reaction rate is now dependent only on the concentration, because k and K are constants of the process.

When applying the equation (6) for the dosing reactor, following dependence is obtained:

$$-V \cdot \frac{dc}{dt} = \frac{m \cdot A \cdot k \cdot K \cdot c}{1 + K \cdot c} \Rightarrow -\frac{m \cdot A}{V} \cdot t = \frac{1}{k \cdot K} \cdot \ln \frac{c}{c_0} + \frac{c - c_0}{k} \quad (10)$$

where V is a volume of fluid, A is a number of adsorption sites per gram of the catalyst and m is a mass of catalyst. From this equation, it is possible to calculate the time needed for reduction of concentration c_0 to $c_0/2$, which is defined as half-time $\tau_{1/2}$:

$$\tau_{1/2} = \frac{\frac{\ln 2}{k \cdot K} + \frac{c_0}{2 \cdot k}}{\frac{m \cdot A}{V}} \quad (11)$$

If the concentration $c_0 \ll 1/K$, the reaction is always of the first order and the half-time does not depend on the initiative reagent concentration c_0 but only on the catalyst concentration (m/V) and its reactivity (k, K).

In some cases, when the reactant is insoluble in water ($c \approx 0$), the reaction is specified by the following equation:

$$v = \frac{d(c_{\text{ads}})}{dt} = -k \cdot (c_{\text{ads}}) \quad (12)$$

The half life of the reaction is than:

$$\tau_{1/2} = \frac{\ln 2}{k} \quad (13)$$

where k is a slope of a linear function $\ln(c_{A0}/c_A) = f(t)$, which runs through zero. Another important parameter for comparing rates of particular reactions is a conversion rate α :

$$\alpha = \frac{c_0 - c_t}{c_0} \quad (14)$$

2.5 Preparation of TiO₂

TiO₂ as a photocatalyst can be used in a form of nanoparticles, nanorods, nanotubes, layers, etc. A wide range of TiO₂ preparation methods is used by titania research teams around the world. As already mentioned before, titania photocatalyst is prepared in a slurry or immobilized form, which is in many cases more convenient than the slurry form. The overall performance of the TiO₂ coating can be affected by various factors depending on the coating methods. In addition, it is also difficult to evaluate the photocatalytic efficiencies of the coatings. Some researches show that TiO₂ could be effective for degradation of certain compounds only. Therefore, there is still a level of uncertainty about which is the most appropriate preparation/deposition method to be used for a particular application.

Typical preparation procedures need to be mentioned: sol-gel process, hydrothermal/solvothermal method, micelle and reverse micelle methods, chemical/physical vapour deposition, electrodeposition, direct oxidation method, microwave method and others. Some of the basic techniques are mentioned below. The chemical vapour deposition technique describes not only titanium dioxide preparation but also its deposition on a substrate. That is why this method is mentioned in the next chapter 2.6.

2.5.1 Sol-gel method

Sol-gel method is one of the methods for preparing photoactive layers. It has many advantages over other methods mainly because of following: no special apparatuses are required; uniform multicomponent films can easily be formed if a homogeneous solution is available; the resultant films are characterized by a porous structure of a gel with a large specific area characteristic.

Sol is a dispersion of solid particles ($\sim 0.1\text{--}1 \text{ mm}$) in a liquid. Sol for TiO₂ film preparation contains a titanium source, alkoxide (e.g. tetraethylorthotitanate, tetrabutyltitanate, titanium tetraisopropoxide). Alkoxides are organometallic compounds of chemical formula $M(\text{OR})_n$, where M stands for a metal and OR is an alkyl group. Alkoxide is then dissolved, usually by an alcohol, which brings water into the system. Water, which is needed for hydrolysis, does not break the solution homogeneity.

The process of TiO₂ preparation, which also includes the sol-gel process, runs in few steps. The whole process will be described on the reactions of tetrabutylorthotitanate $\text{Ti}(\text{OBu})_4$ as a precursor and polyethylene glycol (PEG) as a template. First the complexing reaction

of the $\text{Ti}(\text{OBU})_4$ precursor and the complexing agent diethanolamine takes place. In another step water is added resulting in hydrolysis and polycondensation reaction of $\text{Ti}(\text{OBU})_4$ precursor. Then polyethylene glycol is added into the TiO_2 sol, which plays a role of the structure-directing agent. PEG helps to form an inorganic-organic network, leading to the original morphology of TiO_2 porous films. Finally the TiO_2 sol is deposited on a substrate. The particles in sol are polymerized and produce gel in a state of a continuous network. With further drying and heat treatment (calcination), the remaining organic and inorganic components are pyrolyzed and form an amorphous or a crystalline coating^{12,13,14,15}.

Sol-gel method enables to use titanium isopropoxide as a precursor in ethanol/isopropanol mixture. Hydrochloric acid keeps sol in a homogenous semi-transparent state. Sol clears up after peptisation, a process when dispersion turns into a colloidal state forming clearer sol¹⁹.

2.5.2 Sol-gel method with reverse micelles

In general, micelles are systems created of molecules of surfactants (surface active agents). Each molecule consists of a hydrophilic and hydrophobic part. After reaching the critical micelle concentration (CMC), molecules of surfactant are spontaneously self organized into micelles (aggregates). The shape, size and character of the micelles are influenced by many factors, i.e. structure of the surfactant molecule, system composition, molecular interactions, temperature, etc. The shape and size of the micelles are essentially determined by geometric packing constraints resulting from the shapes and volumes of the lipophilic and the hydrated hydrophilic parts of the amphiphilic molecules.

A simple geometrical model, which explains the influence of the molecular structure of the surfactant on the shape of the micelle, has been defined as a critical packing parameter $CPP = \frac{V}{A \times L}$, where V denotes the volume of the lipophilic part, L the critical lipophilic chain length and A the surface area occupied by the hydrophilic part at the micellar interface. Changing any of the parameters V , L or A is directly reflected in the shape of the micelles. For $CPP > 1$, reversed micelles with negative interface curvature are possible^{16, 17}.

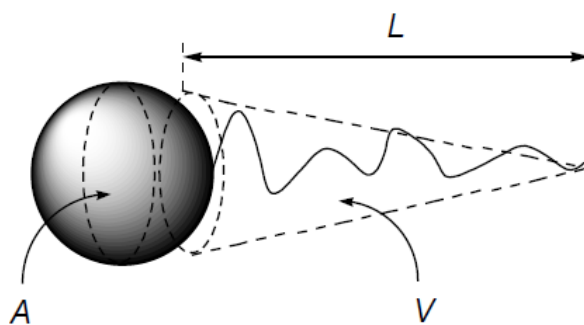


Figure 5 Critical Packing Parameter (CPP)

In non-polar solvent, amphiphilic molecules create reverse micelles reorganised into a shape providing hydrophilic conditions inside the micelle. Due to this arrangement, chemical reactions run in a specified, delimited space which means a limited number of molecules are involved in the reaction and particles of required size are obtained. The reverse micelle system is suitable for catalyzed reactions which run under water conditions. Water is concentrated inside the micelle matrix, so the size and amount of a product can be easily influenced.

Lim et al. prepared emulsion with reverse micelles by mixing Triton-100 surfactant in cyclohexane (solvent) for 30 minutes. The system became turbid after addition of water but cleared up by addition of titanium isopropoxide as the precursor. When stirring, hydrolysis runs in the solution to form a sol of titanium dioxide¹⁹.

Other authors³⁴ studied the influence of the templating agent (surfactant) structure on the crystallographic structure, the size of crystallites, the film thickness or surface homogeneity. The surface roughness is determined by micelle cores. Reverse micelles form identical particles in the core micro-space, which are packed more or less uniformly after removing the template resulting in low extent of surface defects.

2.5.3 Hydrothermal/solvothermal method

This process is conducted in autoclaves under controlled temperature and/or pressure with the reaction in aqueous solutions. The temperature, which can be elevated above the boiling point of water and the amount of solution added to the autoclave largely determine the internal pressure produced.

Many groups have used the hydrothermal method to prepare TiO₂ nanoparticles. For example, TiO₂ nanoparticles were obtained by peptizing (tetraalkylammonium hydroxide as peptizer) the precipitates prepared by adding isopropanol solution of titanium butoxide into deionized water. The peptizers and their concentrations influence the morphology of the particles.

In another example mainly primary structured anatase phase particles without secondary structure were obtained by a reaction of titanium alkoxide in an acidic ethanol-water solution. The size of the particles was controlled by adjusting the concentration of Ti precursor and the composition of the solvent system.

Beside TiO₂ nanoparticles also nanorods, nanowires or nanotubes have been synthesized by the hydrothermal method.

The very similar preparation technique to the hydrothermal method is the solvothermal synthesis differing in used solvents - the solvothermal method uses nonaqueous solvents and in temperature - much higher reaction temperatures are available due to a variety of organic solvents with high boiling points. The crystalline phase and diameter are largely influenced by the precursor/surfactant/solvent weight ratio¹⁸.

2.6 Deposition techniques

Titanium dioxide photocatalyst can be used in few different forms. One of the possible forms is powder. Undoubtedly, there are many advantages of using powder catalyst, on the other hand the powder form is not practical because of the post-treatment separation requirement. mainly because of formation of aggregates⁵. Thereby attempts have been made to immobilize TiO₂ particles in a form of a film.

It can be quite perplexing in determining a suitable immobilisation procedure, particularly if using economical and simple equipment. The overall performance of the TiO₂ coating can be affected by various factors depending on the coating methods. In addition, it is also difficult to evaluate the photocatalytic efficiencies of the coatings as the photocatalytic activity of catalysts is compound specific. The efficiency will vary due to factors such as light source and chemical compounds¹⁹. The aim of many studies is to obtain a suitable immobilization procedure, which involves the determination of suitable combination of coating method and

substrate, prior to the determination of suitable number of coating cycles, calcination duration and temperature. Coatings are evaluated by immobilization efficiency (adhesion and specific deposition, which is average deposition of TiO_2 coating per unit area) and photocatalytic activity.

The films can be deposited on different solid supports as silica, soda lime glass, stainless steel, paper, textiles and other materials. Also the substrate shape effects its performance. Several physical and chemical techniques as sputting, chemical vapor deposition, spray pyrolysis, sol-gel deposition and other can be used to obtain thin films²⁰.

2.6.1 Dip coating

One of the simple deposition techniques is a dip coating process; it can be labelled as the oldest commercial application of sol-gel technology. The first patent on this technology was issued in 1939²¹. It is widely used in laboratories mainly due to the cost savings. The deposition steps are simple to be followed (Figure 6). A substrate is immersed (dipped) to a solution with a precursor and withdrawn vertically from a coating tank with defined velocity. Uniform velocity assures uniform coating. The solvent evaporates and drains along well-defined drying line, where the inorganic species are progressively concentrated by evaporation, leading to aggregation, gelation and final drying to form a type of a dry gel or xerogel. When the substrate speed v_0 and liquid viscosity are low, as is normally the case for sol-gel film deposition, the thickness balances the viscous drag, gravity force and liquid-vapor surface tension.

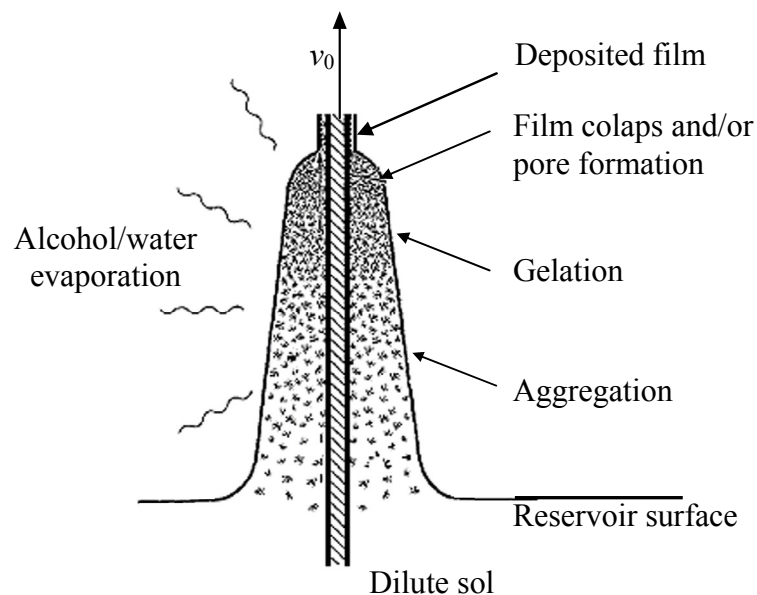


Figure 6 Schematic of steady-state dip-coating process: Sequential stage of structural development

Successful dip-coating requires the condensed phase to remain dispersed in the fluid medium; macroscopic gelation to be avoided and the sol to be sufficiently diluted so that upon deposition the critical cracking thickness is not exceeded^{21, 22}.

2.6.2 Spin coating

Another thin film deposition technique used for several decades is a spin coating technique pictured on the Figure 7. Small amount of a liquid phase depending on the viscosity of the fluid and the size of the substrate to be coated is placed to the centre of a substrate (a) that starts spinning after that (b). Centrifugal acceleration will cause most of the resin to spread to or eventually off the edge of the substrate, leaving a thin film of resin on the surface (d). The solvent evaporates (d), the film is dried and calcinated.

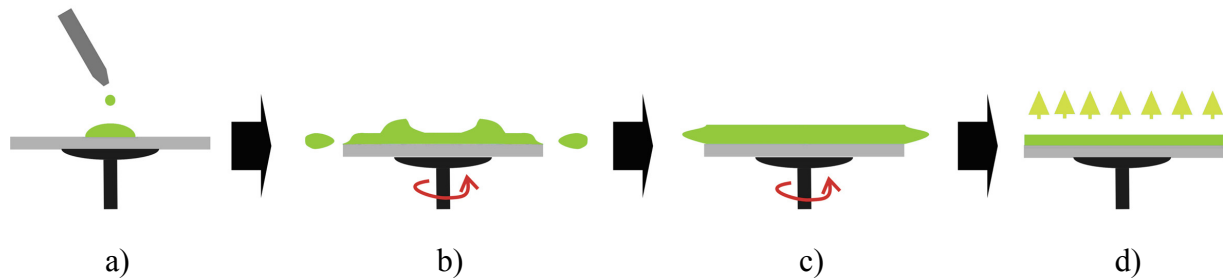


Figure 7 Spin coating deposition technique

Final film thickness and other properties depend on the nature of the liquid media (viscosity, drying rate, percentage of solids, surface tension, etc.) and the parameters chosen for the spin process. Spin speed is one of the most important factors in spin coating. The speed of the substrate (rpm) affects also characteristic turbulence of the air immediately above it. In particular, the high speed spin step generally defines the final film thickness, which is a balance between the force applied to shear the fluid resin towards the edge of the substrate and the drying rate which affects viscosity of the resin²³.

2.6.3 Inkjet printing

Inkjet printing is a non impact dot matrix printing technology in which droplets of ink are jetted from a small aperture directly to a specified position on a media to create an image. Inkjet printing is a very simple technique for preparing a coated substrate, it is widely used in printed electronics because less manufacturing steps are needed, less material waste is produced and also because of cost savings²⁴.

There are two methods for inkjet printing with many variations within each. The first one is a Continual Stream (CS) technique (Figure 8) whereby a continuous ink stream is broken into droplets of uniform size and spacing. An electric charge is impressed upon the drops selectively. The charged drops when passing through an electric field are deflected into a gutter and recirculated while the uncharged drops fly directly to the media to form an image.

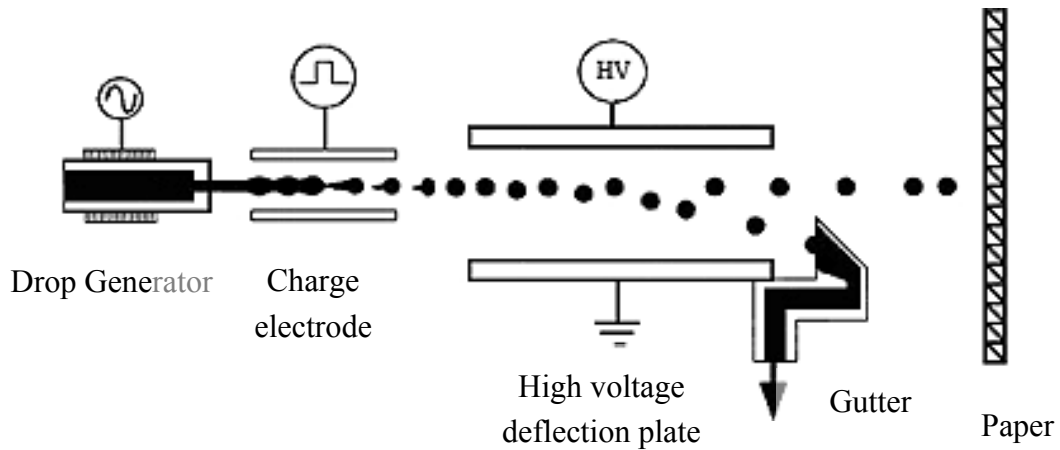


Figure 8 Continual Stream (CS) inkjet printing technique

The second inkjet printing method is a Drop-on-Demand (DOD) technique. DOD technology allows the print head to generate ink droplets only when the drop is needed to create an image on a media. There are four methods of DOD inkjet printing: thermal, piezoelectric, electrostatic and acoustic. Most of the inkjet printers on the markets today use either the thermal (Figure 9) or piezoelectric principal (Figure 10).

Thermal inkjet printing, commonly referred to as bubble jet, is a method where ink drops are ejected from a nozzle by the growth and collapse of a water vapor bubble on the top surface of small heater located near the nozzle^{25,26}. When an ejected ink drop collapses a vacuum is created. This pulls more ink into the print head from the cartridge. Thermal technology is best suited for applications where low ink volumes are required such as home and office.

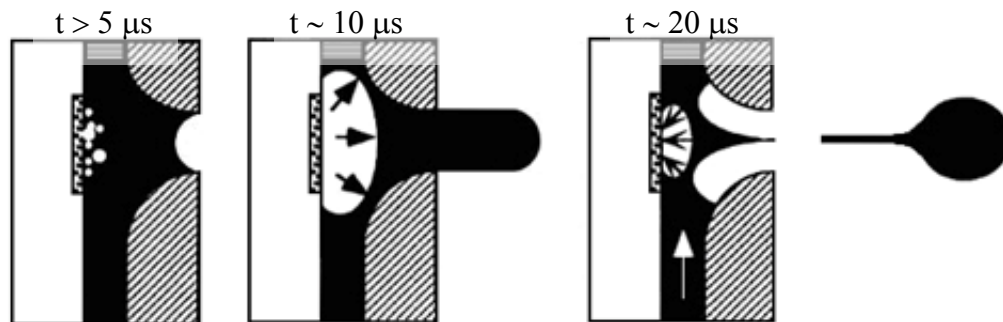


Figure 9 Thermal Drop-on-Demand inkjet printing method

Piezoelectric drop-on-demand printing is patented by Epson. This method uses the deformation of piezoelectric material to cause an ink volume change in the pressure chamber. The piezoceramics receives a tiny electric charge that causes it to vibrate²⁷, which initiates a sudden volume change. The volume change generates a pressure wave that propagates toward the nozzle. This acoustic pressure wave overcomes the viscous pressure loss in the small nozzle and the surface tension force from the ink meniscus so that an ink drop can be ejected from the nozzle.

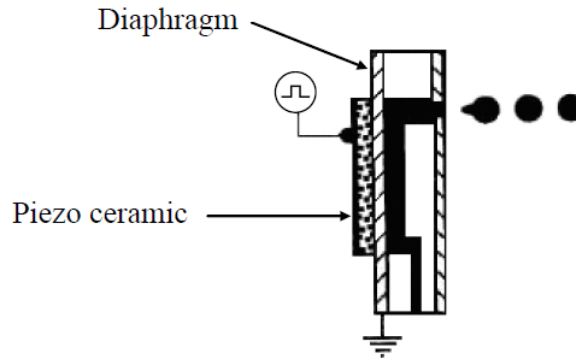


Figure 10 Piezoelectric Drop-on-Demand inkjet printing method

2.6.4 Material printing

Inkjet printing technology enables to use various kinds of inks that mainly need to fulfil ink viscosity and surface tension criteria. This compatibility predicts the inkjet printing to be suitable technology outwith the conventional graphic-arts industry denoted as material printing. The main benefit of the inkjet printing device is precise dosing equipment with precise area location of applied liquid.

All the usable deposition techniques for thin film preparation have their limitations including surface defects liability, non-uniformity of prepared titania films, limited coating area and others. This mentioned problems which come up in process of layer deposition seem to be solved by a promising deposition technique of material printing.

2.6.4.1 Material printing applications

The term „material printing“ refers to the material deposition by inkjet printing where traditional ink is replaced by liquid media, which can be printed on various kinds of substrates. Compared to other deposition techniques, material printing is very accurate method that enables direct patterning. Both thermal and piezoelectric printheads can be used to focus the liquid media droplets on a specified place of the substrate. Material printing enables accurate overprinting if more than one layer is required to be applied. A complicated structure composed of various functional materials can be compared to the conventional planar deposition techniques. The major and very important difference includes the fact that the material printing produces compositions by focused deposition of liquid media on a substrate without any mask. The final composition can be in a form of a homogeneous layer or local deposited areas (2D). Also printing of 3D patterns is not an unrealizable task nowadays.

One of the very first applications of material printing was preparation of printed electrical conductive patterns. Previous preparation techniques as serigraphy where printing matrix needs to be prepared are more complicated. Also the material printing way had one major problem – composition of the applied ink, which tended to coagulate. After this problem was solved more complicated active and passive electronic parts or optoelectronic devices (OLED, LCD displays) were prepared.

Bio-structures as proteins or nucleic acids are also suitable structures for material printing technique. In another case if a suitable composition of printing liquid precursor is applied, also ceramic layers can be prepared by material printing²⁸.

2.6.4.2 Specialized printing device

There are two groups of printing devices, which can be used for material printing, common inkjet printing devices and specialized ones. The applicant always has to balance between price and function. The major advantage of the specialized equipment is a precise control upon the overall printing process enabled by its software. Common consumer printers can never achieve the precision of the specialized printing devices, on the other hand the price of the printers is many times lower²⁸.

FUJIFILM Dimatix can be mentioned here as a specialized piezoelectric drop-on-demand ink jetting technology that develops high performance, micro-precision printheads and systems for depositing picoliter sized droplets of fluids, such as liquid silver and organic "inks", on all types of surfaces, including flexible substrates, flat panel and flexible displays, printable electronics, bioscience and a wide variety of other applications. This technique covers the needs of material printing and enables micro-production processes that are extremely cost effective, much less wasteful and more economical in small production volumes.

The Dimatix material printer (Dimatix Materials Printer DMP-2800) can create and define patterns over an area of about 200×300 mm and handle substrates up to 25 mm thick with an adjustable height. The temperature of the vacuum platen, which secures the substrate in place, can be adjusted up to 60 °C. The printer offers a variety of patterns by employing a pattern editor program. Additionally, a drop-watch camera system allows manipulation of the electronic pulses to the piezo jetting device for optimization of the drop characteristics as it is ejected from the nozzle. There is a built-in cleaning station that includes an automatic capping mechanism. This system thereby enables easy printing of structures and samples for process verification and prototype creation. The cartridge-style printhead allows users to fill their own fluids and print immediately with the printer in their own laboratory. To minimize waste of expensive fluids, each cartridge reservoir has a capacity of 1.5 ml. Cartridges can easily be replaced to facilitate printing of a series of fluids. Each single-use cartridge has 16 nozzles linearly spaced at 254 microns with typical drop sizes of 1 and 10 picoliters²⁹.

2.6.5 Chemical vapour deposition

Vapour deposition refers to any process where materials in vapour state are condensed to form a solid-state material. These processes are commonly used to form coatings to alter the mechanical, electrical, thermal, optical, corrosion or wear resistance of various substrates. They are also used to form fibres, films and composite materials. Vapour deposition processes usually take place within a vacuum chamber. If no chemical reaction occurs, this process is called Physical vapour deposition (PVD), otherwise, it is called Chemical vapour deposition (CVD), where thermal energy heats the gases in the coating chamber and drives the deposition reaction.

In addition, various CVD approaches are used in preparing TiO₂ nanomaterials, such as electrostatic spray pyrolysis, thermal plasma pyrolysis, diffusion flame pyrolysis, laser-induced pyrolysis, among others¹⁹.

2.7 Aspects effecting the TiO₂ film structure

In majority of TiO₂-coating applications accessibility to a crystalline surface is of prime importance. Therefore the production of an open, highly porous titanium dioxide network in either the anatase crystalline phase is desirable because (1) the high surface area allows

maximum contact between the TiO₂ network and the reaction medium and (2) the continuity of the network prevents traps from depleting its efficiency. The preparation of thin films with good control of pore size distribution and without delamination or cracking in the calcination process is technically challenging but there have been a few successful examples. The success in obtaining a specific mesoporous metal oxide depends on two factors: (1) the occurrence of a three-dimensional mesophase and (2) the stability of the metal oxide framework upon the removal of the surfactant species³⁰.

2.7.1 Effect of calcination temperature and calcination time

Two different methods of heat treatment are usually used if more layers are deposited: (1) annealing of each layer at a temperature sufficient for crystallization of the film or (2) drying of the titanium oxide film mostly at 100–150 K after each layer deposition in order to remove the solvent and subjecting to high-temperature heat treatment only after the deposition of the last layer. Kuznetsova et al. studied these two approaches and said that a large number of cavities in the sample can be due to the prolonged drying resulted in the solvent evaporation before the high-temperature treatment. Evaporation of the solvent from the gel film affects the morphology. A sol film is required to have a sufficient fluidity for some time during the drying process to form macroporous structure. As prepared film is porous not only on the surface but also in the bulk, so the film is thick enough to make possible the formation of a three-dimensionally interconnected sponge-like pore structure³¹.

Taichen et al. found that an increase in the treatment temperature results in an increase in the crystallinity. The mean crystalline size increased from 9.8 to 36 nm when the treatment temperature was increased from 350 to 650 °C. The pore size is the smallest at 350 °C-calcinated sample. The pore size is higher with increasing calcination temperature, which is due to the mesoporous structure consolidation as a result of improved crystallinity. It was also observed that for the sample calcined at 650 °C aggregates of plate-like structure exist and that the mesoporous structure is completely collapsed, nonporous³².

Arconada et al. studied the evolution of crystalline fraction as a function of temperature and time of the heat treatment. An important increment is observed for short treatments, associated with the rapid formation and/or growing of anatase crystals. Above 3 hours of heat treatment, the crystalline fraction maintains quite constant for $T \geq 400$ °C. Coatings treated at 350 °C need a longer time (10 hours) for total crystallization³³.

They also explained the relation between the coatings thickness and the calcination temperature and time. The coating thickness decreased with temperature and time of the thermal treatment due to the concentration of the network associated with the sintering process.

Other relevant property related with photocatalytic activity is the specific surface area S_S . At 350 °C low S_S are observed probably due to the incomplete removal of organic residues, still present in the structure. Above this temperature, S_S increases up to the maximum situated around 400–450 °C. Higher treatment temperatures reduce the photoactivity of the coatings.

These results indicate that the photoactivity of titania coatings is closely related with S_S . Although the presence of anatase is necessary, the crystal fraction and crystal size seem not to play a critical role in photocatalyst behavior. These conditions implicate a compromise in temperature and time of sintering to ensure the appearance of TiO₂-anatase crystal phase, maintaining the high porosity of the layer³³.

Guo et al. also proposed results of thermal analysis of TiO₂-PEG composites as weight losses against temperature. The first weight loss at temperatures below 100 °C was clearly

the removal of physisorbed water. The second weight loss between 200 and 300 °C could be attributed to the expulsion of organics. The removal of structural water came in last between 300 and 400 °C with subsequent increase in the number of bridging oxygen and thus the monolithic nature of the gel matrix. The presence of PEG in the xerogel had apparently raised the temperatures of corresponding weight loss events in the PEG-free xerogel. As result, the gel became more thermally stable with the increase in the PEG content¹⁵.

2.7.2 Substrate and coating solution

Lim et al. studied, among other issues, relation between substrate and applied coating solution. The used substrates were fibreglass, woven fibreglass, aluminum plate and glass slide. The best immobilisation efficiency provided fibreglasses as they have a relatively large effective surface area compared to smooth glass slides. The most suitable solutions are viscous coating solutions as combination of sol-gel solution enriched with TiO₂ powder (Figure 11). On the other hand, they have high tendency to detach.

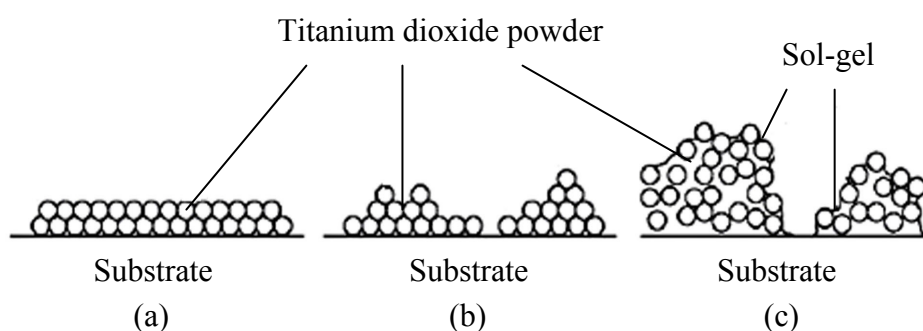


Figure 11 Illustration of TiO₂ coating arrangement for (a) ideal coating, (b) slurry coating and (c) hybrid coating

2.7.3 Role of the template molecular structure

Molecular templating in the sol-gel process represents a unique approach in production of uniform particles efficient as parts of sensors and other electrochemical devices³⁴. The series of titania thin films produced under otherwise the same conditions but varying in the molecular structure of templates were studied. The practical importance is to be able to design optimized films for photo-responding purpose.

In the case of sol-gel method carried out in reverse micelle system the templating structure provides not only the shape to the forming particles but also a well defined microspace for a series of reactions. In each micro-vessel only a limited number of molecules react forming uniform particles. Using structurally similar templates differing only in some characteristic moieties predict the ability to imprint variable functionality to the organized matter of the identical chemical composition.

Morozova et al. used reverse micelle sol with five types of non-ionic surfactant Triton X differing in the number of oxyethylene groups (OXG) of the hydrophilic non-polar chain. The general name Tritons for the group of non-ionic surfactants of the (p-(1,1,3,3-tetramethyl)phenyl)poly(oxyethylene) type comes from water lizards bearing Latin names *Tritonus vulgaris* and *Tritonus alpestris*. Their bodies with a short, but large head and a long tail resemble the hydrophobic and hydrophilic parts of these molecules (Figure 12).

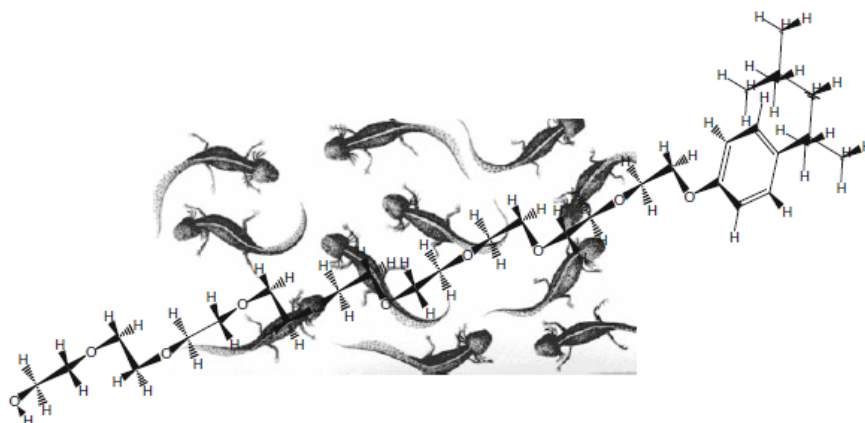


Figure 12 Typical structure of the Triton X surfactant type

Very important variable in the reverse micelle system is the ratio $R = \text{solvent/surfactant/water/precursor}$. Water molecules are dominantly associated with the $-\text{OH}$ groups of the hydrophilic chain. It is obvious that the kinetics of hydrolysis inside of reverse micelle core is enabled by water molecules necessary for the complete hydrolysis of the titanium precursor (titanium isopropoxide).

For all prepared layers anatase form was achieved. With the increasing number of OXG crystallinity of the layers increased as well. The shortest template created amorphous material; the longer chains of templates gave well developed crystallinity. All the prepared layers were transparent and mechanically resistant³⁴.

2.7.4 Number of coating cycles

The important variable for thin TiO_2 layers preparation is definitely the film thickness as a function of number of deposition cycles. It is observed that the film thickness is a function of the used templating (surfactant) environment. In the environment of reverse micelle sol longer hydrophilic chains of the template caused thicker layers.

2.8 Pre-treatment of soda-lime glass support

One of the suitable substrates that are widely used for thin film deposition is soda-lime glass. When a transparent thin film of titanium dioxide is formed on a surface, an organic compound containing titanium is thermally decomposed. The temperature is raised to about $400\text{ }^\circ\text{C}$ so that a hard film of titanium dioxide can form on the glass support. However, if the temperature is raised too far, the soda-lime glass begins to soften and the sodium ions slowly diffuse from the glass and form a sodium-titanium-oxygen compounds, which do not provide photocatalytic reactions.

Sodium diffusion needs to be blocked. One of the successful methods is application of silicon dioxide (pure silica glass) layer as a pre-coat. Another possibility is to acid the glass substrate, in other words, to boil the glass substrate in acid, mostly in hydrochloric acid (HCl) or sulfuric acid (H_2SO_4)³⁵.

2.9 Chemical reactors

The type of used reactor depends on the physical properties and chemical reactivity of the substances that come into the reaction. If a reactor for photocatalytic reaction is used,

the selection of the reactor material is very important. Photons are present at the photocatalytic reaction, so the radiation has to pass through the reactor material without any loss of intensity. The irradiation spectrum should be equal to the absorption spectrum of the photocatalyst. If a semiconductor photocatalyst is used, the energy of the absorbed radiation should be equal or higher than the energy of the semiconductor bandgap.

The reactors can be divided according to the movement of the reaction mixture inside the reactor. Continuous (flow) reactors use continuous feeding of a substance and also continuous withdrawing of a product which makes the mass inside the reactor circulate. On the other hand, if a reactant is dosed at the beginning of the reaction and a product is withdrawn at the end of the reaction, we talk about discontinual (batch) reactors^{9,36}.

2.10 Characterization of TiO₂ films

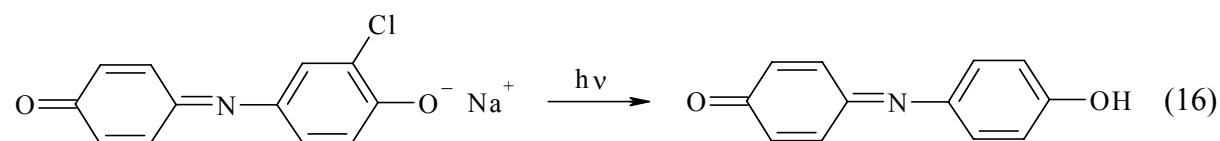
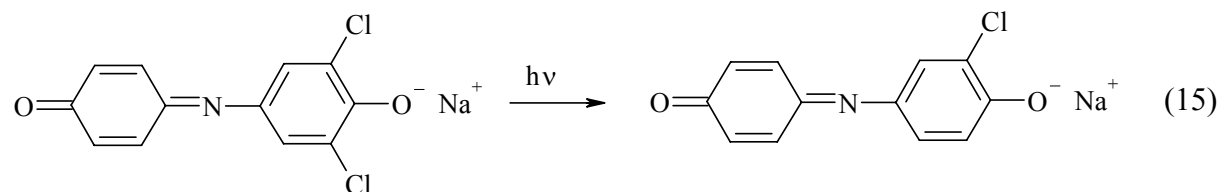
The thin films of anatase titania on glass supports are sold world-wide by glass manufacturers for their semiconductor photocatalytic behaviour of the complete oxidative mineralization of organic pollutants in water and air purification. The films are also more easily wetted by water after UV irradiation. Although it remains unclear how UV-induced hydrophilicity and photocatalysis are related. It is clear that any titania film which is photocatalytically active also exhibits UV-induced hydrophilicity.³⁷

A set of methods can be used to describe and compare titania thin films by demonstrating their photocatalytic behaviour and photoinduced hydrophilicity.

2.10.1 Photocatalytic activity of TiO₂ films

2.10.1.1 Photocatalytic oxidation of 2,6-dichloroindophenole

Following mechanism was suggested by Brezova et. al for the mechanism of destruction of 2,6-dichloroindophenol that was used in the study of kinetics of photocatalytic process on the TiO₂ photocatalyst³⁸:



The process was described as a dechlorination in steps. The molecule of DCIP is complicated, which means also the degradation process will be complicated including a number of competitive synthesis, in this case some less complicated molecules as formic acid are more suitable. The process of DCIP degradation is monitored via the UV-VIS spectrometry. Also visual observation of the degradation process progress can be done, as the solution of DCIP changes from violet to pink color.

2.10.1.2 Photocatalytic degradation of stearic acid

The stearic acid (SA) test is a simple method for assessing the activities of titania photocatalyst films. The test involves the initial deposition of a thin layer of SA onto the active layer under test and the subsequent monitoring of its photocatalytic destruction under defined conditions as a function of time. This reaction is preferred for a number of reasons – SA is very stable under UV illumination in the absence of photocatalyst; SA films are easily laid down from an organic solvent solution (methanol, chloroform, isobutyl alcohol); the kinetic of stearic acid degradation is usually simple and zero-order and there are many methods by which the mineralization process can be monitored. The overall reaction can be summarized as described in equation (17).



The most often used method for studying this reaction is via the degradation of SA film using infrared absorption spectroscopy. SA absorbs strongly in the region 2700–3000 cm^{-1} with peaks at 2958 cm^{-1} due to asymmetric in-plane C–H stretching in CH_3 group and with peaks at 2923 cm^{-1} and 2853 cm^{-1} describing asymmetric and symmetric C–H stretching in CH_2 groups, respectively. The integrated area due to these peaks over the range 2700–3000 cm^{-1} is proportional to the amount of stearic acid present. The FT-IR spectra describe a function of absorbance versus wavenumber as a function of irradiation time.

Mills et al. has reported³⁷ that sol-gel produced titania films are able to remove completely a SA covering layer via semiconductor photocatalysis. Their work shows that no major intermediates, volatile or otherwise, are generated via the photocatalytic mineralisation of SA film; the only major and readily observed IR active species present during the course of the photomineralization process are SA and CO_2 .

Evans et al. in his study described the relation between the stearic acid test and contact angle results. The group of co-workers suggested that photocatalytic activity of the films when determined by the stearic acid test is directly related to the contact angle performance. Their obtained results provided an interesting evidence to support the explanation of the mechanism behind photo-induced superhydrophilicity (PSH) observed on the surface of TiO_2 thin films. Their theory relates PSH to the ability of the material to photo-mineralize surface organics, resulting in a “clean” surface and hence enhanced wettability. The ability of the surface to degrade organic pollutant (i.e. SA) is directly related to its ability to show PSH upon band gap irradiation.

2.10.2 Contact angle measurement

Measurement of contact angle provides a better understanding of the interactions between phases, regardless of whether they are gas, liquid or solid. The wettability and surface energy of solid surfaces plays an important role in many processes, such as controlled capillary action, spreading of coatings, adhesion and absorption into porous solids etc. Contact angle is a rapid and accurate characterization tool.

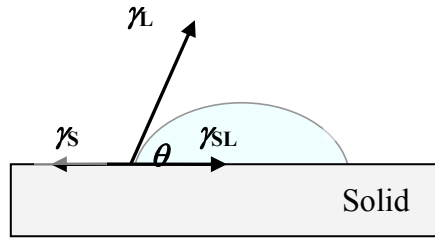


Figure 13 Interface/surface tensions between liquid and solid

Contact angle is a quantitative measure of the wetting of a solid by a liquid. It is a direct measure of interactions taking place between the participating phases. The degree of wetting (wettability) is determined by a force balance between adhesive and cohesive forces. Adhesive forces between a liquid and solid cause a liquid drop to spread across the surface. Cohesive forces within the liquid cause the drop to ball up and avoid contact with the surface.

Contact angle is geometrically defined as the angle on the liquid side of the tangential line drawn through the three phase boundary where a liquid, gas and solid intersect.

The shape of the drop and the magnitude of the contact angle are controlled by three interaction forces of interfacial tension of each participating phase (gas, liquid and solid) (Figure 13). The relation between these forces and the contact angle can be evaluated by the Young's equation³⁹:

$$\gamma_L \cos \theta = \gamma_S - \gamma_{SL} \quad (18)$$

where θ is a contact angle, γ_S , γ_L , γ_{SL} are solid surface, liquid surface and solid/liquid interfacial free energy, respectively.

In the case that $\gamma_S \geq \gamma_L + \gamma_{SL}$ liquid is spread over the surface to form energetically more convenient state. This situation with zero contact angle can be defined as superhydrophilicity. On the other hand, if $\gamma_S < \gamma_L + \gamma_{SL}$, liquid does not spread over the surface but creates a shape of a drop, characterized by a contact angle. According to a degree of wetting, following cases are defined⁴⁰:

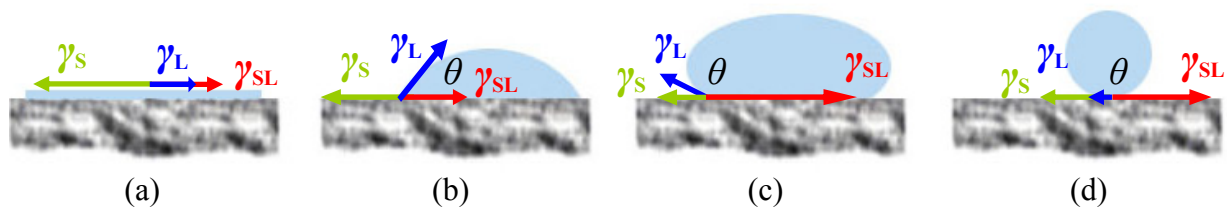


Figure 14 Different wetting ability of solid substrates

(a)	$\gamma_S = \gamma_L + \gamma_{SL}$	$\theta = 0^\circ$	perfect wetting
(b)	$\gamma_S > \gamma_{SL}$	$0^\circ < \theta < 90^\circ$	high wettability
(c)	$\gamma_S < \gamma_{SL}$	$90^\circ < \theta < 180^\circ$	low wettability
(d)	$\gamma_S = \gamma_{SL} - \gamma_L$	$\theta = 180^\circ$	perfectly non-wetting

Contact angles values obtained by measurement can be influenced by surface contamination, impurities by presence of adsorbed gas molecules or by possible interactions between solid phase and liquid phase (chemical reaction, dissolving or swelling). To summarize this topic an ideal solid surface is the one that is flat, rigid, perfectly smooth, and chemically homogeneous and has zero contact angle hysteresis. For this kind of ideal surface, Young's equation is applied to count a contact angle.

2.10.2.1 Photo-induced hydrophilicity

A thin film composed of titanium dioxide photocatalyst combined with suitable additives shows an initial contact angle for water of several tens of degrees. When exposed to UV light, water starts to exhibit a decreasing contact angle; it tends to spread out flat. The best hydrophilic surface is that of zero contact angle, meaning that water spreads perfectly across the surface. At this stage the surface becomes completely non-water-repellant and is said to be superhydrophilic.

The surface retains a contact angle of few degrees for water for a day or two without being exposed to ultraviolet light. Then the contact angle slowly increases and the surface becomes hydrophobic again. The superhydrophilicity can be recovered simply by exposing the surface to the UV light again⁶.

Also other liquids as glycerol trioleate, hexadecane, ethylene glycol or tetralin were used to measure contact angle. It was discovered that all mentioned liquids spread out, from which we conclude that UV illumination creates amphiphilic titania surface.

Photo-induced hydrophilicity is at present attributed to the production of "oxygen defects" on the surface of the titanium dioxide. Oxygen atoms are ejected and these photoinduced oxygen vacancies are replaced by dissociated water molecules, resulting in hydrophilic surface (Figure 15). One of the benefits of superhydrophilicity is the fact that, as the surface is less likely to form water droplets, it dries quickly. This effect occurs on indoor glass panels, where the formation of dew (usually in winter) can be prevented.

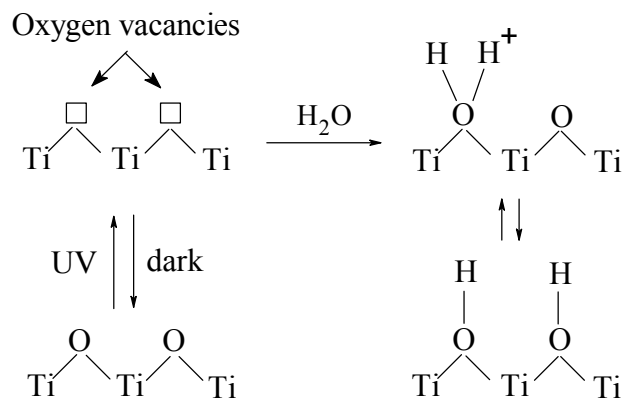


Figure 15 Mechanism of photoinduced hydrophilicity

2.10.3 Band gap determination

Light absorption and emission in a semiconductor is known to be heavily dependent on the detailed band structure of the semiconductor. The band gap represents the minimum energy difference between the top of the valence band and the bottom of the conduction band. However, the top of the valence band and the bottom of the conduction band are not generally at the same value of the electron momentum (wavevector), so direct and indirect band gap semiconductors are distinguished.

In a direct band gap semiconductor the top (maximum) of the valence band and the bottom (minimum) of the conduction band occur at the same value of momentum. The conduction and valence band are vertically aligned. Absorption of a photon is obtained if an empty state in the conduction band is available for which the energy and momentum equals that of an electron in the valence band plus that of the incident photon.

Indirect band gap semiconductors, for which the minimum of the conduction band does not occur at the same wavevector as the maximum of the valence band, are known to have a smaller absorption coefficient. For an indirect band gap semiconductor, the conduction band is not vertically aligned to the valence band. Therefore a simple interaction of an incident photon with an electron in the valence band will not provide the correct energy and momentum corresponding to that of an empty state in the conduction band. As a result, absorption of light requires the help of another particle – phonon (lattice vibration). Phonon has a small energy and large momentum compared to that of a photon. Photon absorption in indirect band gap semiconductors can then occur by absorption or emission of a phonon.

Since the absorption process in an indirect band gap semiconductor involves interaction of three particles (a phonon, an electron and a photon), the probability of such interaction will be lower than a simple electron-photon interaction in a direct band gap semiconductor. As a result it is clear that absorption is much stronger in a direct band gap material. The same principle applies to light emission, recombination of electrons and holes to produce photons. Direct band gap material is also more likely to emit a photon than an indirect band gap material.

As a result of such considerations, direct band gap semiconductors are used to make optical devices such as LEDs and semiconductor lasers, whereas an indirect band gap semiconductor is not⁴¹⁻⁴².

Band gap energy can be evaluated from the reflectance spectra of a powder form semiconductor material. The reflectance spectra are analyzed using Kubelka-Munk formalism to convert the reflectance into the equivalent absorption coefficient, according to

$$\alpha_{KM} = \frac{(1 - R_{\infty})^2}{2R_{\infty}} \quad (19)$$

where R_{∞} is the reflectance of an infinitely thick sample with respect to a reference at each wavelength. Indirect and direct band gap semiconductors follow the relations (20) and (21), respectively⁴³.

$$(\alpha_{KM} \cdot h\nu)^{\frac{1}{2}} = f(E) \quad (20)$$

$$(\alpha_{KM} \cdot h\nu)^2 = f(E) \quad (21)$$

Extrapolation of the reflectance versus wavelength/energy curves determines the band gap energy (absorption edge). According to a study lead by Reyes-Coronado et al., the above method was used to calculate the band gap of anatase, rutile and brookite pure phases in powder form. Their measurements resulted in values of band gap energies of 3.00 eV for rutile, 3.13 eV for brookite and 3.21 eV for anatase, as is in agreement with literature. In general, the measurement of optical properties of metal oxide nanopowders at room temperature is complicated by superposition of a large number of transitions. In the case of

anatase there is a consensus that the absorption edge is around 3.2 eV, associated with indirect transitions⁴.

2.11 Instruments for TiO₂ films characterization

2.11.1 UV/VIS spectrophotometry

UV/VIS spectrophotometry is used to determine the absorption or transmission of UV/VIS light by a sample. It can also be used to measure concentrations of absorbing materials based on developed calibration curves of the material.

The UV/VIS spectrophotometer is employed to measure the amount of light that sample absorbs. It uses two light sources, a deuterium (D₂) lamp for ultraviolet light and a tungsten (W) lamp for visible light. The light beam passes through a group of slits and mirrors, after that it splits into two beams. One of the beams is allowed to pass through a reference cuvette with solvent, the other passes through the sample cuvette. The intensities of the light beams are then measured at a detector.

The change in intensity of light dI after passing through a sample should be proportional to the path length db [cm], concentration c [mol·dm⁻³] of a sample and intensity of the incident light I . Thus, dI is proportional to $b \cdot c \cdot I$:

$$\frac{dI}{I} = -k \cdot c \cdot db \quad (22)$$

$$-\int_{I_0}^I \frac{dI}{I} = k \cdot c \cdot \int_0^b db \quad (23)$$

where k is proportionality constant, I_0 is the initial intensity of the beam before entering the sample. Integration of this equation leads to Lambert-Beer law:

$$-\ln \frac{I}{I_0} = k \cdot b \cdot c \quad (24)$$

$$A = -\log \frac{I}{I_0} = \varepsilon_\lambda \cdot b \cdot c. \quad (25)$$

where $\varepsilon_\lambda = 2,303 \cdot k$ is a molar absorption coefficient [dm⁻³ · mol⁻¹ · cm⁻¹]. A is defined as absorbance and is directly proportional to the path length b and the concentration of the sample c . The molar absorption coefficient is characteristic of the substance under study and is a function of the wavelength. Molecules strongly absorb only in some regions of electromagnetic spectrum. The photon carries a specific amount of energy defined by its wavelength. The least energy of photon (the longest wavelength) corresponds to the energy difference between the ground and the first excited state (or promotion of an electron from the highest filled orbital to the lowest unfilled orbital).

2.11.2 Optical microscopy/Digital microphotography

Optical microscopy refers to the inspection of the sample at higher magnification using an optical/light microscope. Low-power microscopes typically magnify the specimen at 5× to 60× (100×). High-power microscopes, on the other hand, typically magnify the specimen up to 1000×. During the inspection, the specimen is positioned perpendicularly to the axis of the objective lens. Light is then shown on the sample, which reflects some light back

to the lens. The image seen in the microscope depends not only on how the specimen is illuminated and positioned, but on the characteristics of the specimen as well⁴⁴.

A basic microscope contains following parts: a lamp to illuminate the sample, a nose piece to hold objectives used to change viewing magnification, a field diaphragm to adjust the field of view, an eye piece to magnify the objective image and a stage for manipulating the sample.

Three modes out of a wide range of the contrast enhancing techniques commonly used in optical microscopy are mentioned here - brightfield illumination, darkfield illumination, and interference contrast (Nomarski). The mode of operation must be chosen well to meet the desired results⁴⁵.

Bright field mode of viewing an object provides the most uniform illumination of the sample; a full cone of light is focused by the objective on the sample. The image observed results from the various levels of reflectivities exhibited by the compositional and topographical differences on the sample surface.

Under darkfield illumination, the sample is only illuminated by light that impinges on its surface at a glancing as the inner circle area of the light cone is blocked. This scattered reflected light usually comes from feature edges, particulates and the other irregularities on the sample surface. Darkfield illumination is therefore effective in detecting surface scratches and contaminations.

Polarized light that is divided by Wollaston prism into two orthogonal light packets is used in interference contrast mode. The slightly displaced light packets hit the specimen at two different points and return to the prism through different paths. The differences in the routes of the reflected packets will produce interference contrasts in the image when the packets are recombined by the prism upon their return. Surface defects or features such as etch pits and cracks that are difficult to see under brightfield illumination can stand out clearly under Nomarski mode⁴⁴.

Digital microphotography is a way to record and maintain images. The quality of the photography depends on the quality of the microscopy. Microscope configuration errors represent the greatest issue to quality photomicrographs, followed by errors in filter selection, film choice, aberration, dirt and processing mistakes. When properly adjusted, the microscope will yield images that have even illumination over the entire field of view and display the best compromise of contrast and resolution.

The primary medium for photography was film until the past decade when improvement in electronic camera and computer technology made digital imaging cheaper and easier to use than conventional photography. The cameras operate by capturing the image projected directly onto a computer chip. Digital images offer many opportunities for computer control image manipulation and enhancement as well as the advantage of permanence of digital storage⁴⁶.

2.11.3 FT-IR spectrometry

Fourier Transform InfraRed spectrometry (FTIR) is a tool for identifying types of chemical bonds in a molecule by producing an infrared absorption spectrum. This method can be applied to the analysis of solids, liquids, and gasses for identifying types of chemical bonds (functional groups) where the wavelength of infrared light from the range of $1280-10\text{ cm}^{-1}$ absorbed is characteristic of the chemical bond. While organic compounds have very rich, detailed spectra, inorganic compounds are usually much simpler. For most common materials, the spectrum of an unknown sample can be identified by comparison to a library of known compounds.

The principle of the method is the absorbance of infrared light by passing through a sample causing change in rotation and vibration energy states of molecules. The obtained FTIR spectrum describes dependence of energy, expressed usually by transmittance or absorbance, on the wavelength or wavenumber. Absorption bands with peaks in the interval of $4000\text{-}1500\text{ cm}^{-1}$ are suitable for identification of functional groups (e.g. -OH , C=O , N-H , CH_3). Absorption bands with peaks in the interval of $1500\text{-}400\text{ cm}^{-1}$ are called “fingerprints” (fingerprint region)⁴⁷.

FT-IR spectrometers are often simply called FT-IRs. But for the purists, an FT-IR is a method of obtaining infrared spectra by first collecting an interferogram of a sample, which has the unique property that every data point (a function of the moving mirror position) which makes up the signal has information about every infrared frequency which comes from the source. The measured interferogram signal is “decoded” to obtain a frequency spectrum via Fourier Transformation (FT). An FT-IR Spectrometer collects and digitizes the interferogram, performs the FT function and displays the spectrum⁴⁸.

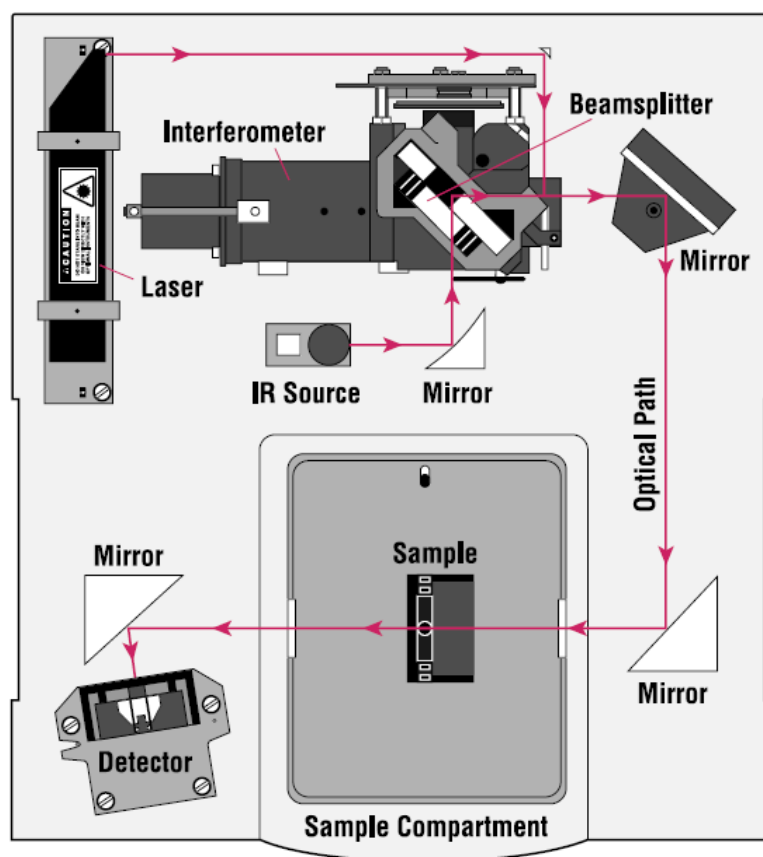


Figure 16 A simple spectrometer layout

The instrumental process is as follows (Figure 16). The source emits infrared energy from a glowing black-body source. This beam passes through aperture which controls the amount of energy presented to the sample. The beam enters the interferometer where spectral encoding takes place resulting in interferogram. The beam enters the compartment where it is transmitted through or reflected off of the surface of the sample, depending on the type of analysis being accomplished. This is where specific frequencies of energy, which are uniquely characteristic of the sample, are absorbed. The beam finally passes to the detector for

final measurement. The detectors used are specially designed to measure the special interferogram signal. The measured signal is digitized and sent to the computer where the Fourier transformation takes place to obtain the final infrared spectrum⁴⁹.

2.11.4 Scanning electron microscopy

Scanning electron microscope is designed for direct studying of the surfaces of solid objects. The scanning electron microscope (SEM) uses a focused beam of high-energy electrons to generate a variety of signals at the surface of solid specimens. The signals that derive from electron-sample interactions reveal information about the sample including external morphology (texture), chemical composition, crystalline structure and orientation of materials making up the sample⁵⁰.

A beam of electrons is produced at the top of the microscope by heating of a metallic filament. The electron source is called "gun". The electron beam follows a vertical path through the column of the microscope. It makes its way through electromagnetic lenses which focus and direct the beam down towards the sample. When a SEM is used, the column and sample must always be at vacuum⁵¹.

Accelerated electrons carry significant amount of kinetic energy and this energy is dissipated as a variety of signals produced by electron-sample interactions when the incident electrons are decelerated in the solid sample. These signals include secondary electrons (that produce SEM images), backscattered electrons, diffracted backscattered electrons (to determine crystal structures and orientations of minerals), photons (X-rays used for elemental analysis), visible light and heat.

Secondary electrons and backscattered electrons are commonly used for imaging samples: secondary electrons are most valuable for showing morphology and topography on samples and backscattered electrons are most valuable for illustrating contrasts in composition in multiphase samples. SEM analysis is considered to be "non-destructive", so it is possible to analyze the same materials repeatedly.

SEMs always have at least one detector (usually a secondary electron detector) and most have additional detectors. The specific capabilities of a particular instrument are critically dependent on which detectors it accommodates. High-resolution images of shapes of objects are displayed to show spatial variations in chemical compositions as the measurement output⁵¹.

Many SEM applications require minimal sample preparation, depending on the nature of the samples and the data required. Samples must be solid and they must fit into the microscope chamber. An electrically conductive coating must be applied to electrically insulating samples for study in conventional SEM's. Most electrically insulating samples are coated with a thin layer of conducting material, commonly carbon, gold or some other metal or alloy. The choice of material for conductive coatings depends on the data to be acquired: carbon is most desirable if elemental analysis is a priority, while metal coatings are most effective for high resolution electron imaging applications. Alternatively an electrically insulating sample can be examined without a conductive coating in an instrument capable of "low vacuum" operation⁵¹.

3 EXPERIMENTAL

3.1 Chemicals, devices and software

3.1.1 Chemicals

- Sodium 2,6-dichloroindophenolate hydrate (DCIP), A.C.S. reagent, Aldrich
- Titanium(IV)isopropoxide (TTIP), Purum, Fluka
- Xylene, p. a., Penta, Czech republic
- Triton X 102, Sigma-Aldrich
- Stearic acid
- Sulfuric acid p.a., min. 93%, Lachema, Neratovice
- Demineralized water

3.1.2 Devices

- Analytical scales Scaltec, SPB 32
- Density Meter DMA 4500. Anton Paar
- Automated Micro Viscometer AMVn, Anton Paar
- Dimatix Materials Printer DMP-2800
- Annealing furnace ELSKLO
- Contact Angle System OCA 10, DataPhysics
- Metal-halide lamp Philips HPA 400/30 SD
- Lamp Osram HQL 125 W
- Radiometer X 97 with Radiometric Detector Head, Gigahertz-Optic
- Continuous reactor with rotary sample holder
- Pumping device PCD 83
- Magnetic stirring device, Lavat Chotutice
- UV-VIS Spectrophotometer Spectronic Unicam, Helios α
- Red Tide USB650 Fiber Optic Spectrometer, Ocean Optics
- Certified reflectance standard Labsphere
- Optical microscope Nikon Eclipse E200
- Digital camera Nikon D5000
- FT-IR spectrometer Nicolet Impact 400
- Electron microscope MIRA II LMU, Tescan

3.1.3 Software

- Microsoft Excel 2003
- Microsoft Word 2003
- Origin, version 7.5
- Adobe Photoshop Lightroom, version 2.6
- Adobe Photoshop CS2
- Camera Control Pro

- SCA20, version 3.5
- SpectraSuite, Ocean Optics
- Vision Scan, version 3.5
- Omnic software

3.2 Titanium dioxide film deposition

3.2.1 Substrate pretreatment

Soda-lime glass (50×50×1.1 mm, Merci, Czech Republic) was used as a substrate for the TiO₂ film deposition. The glass plates were boiled in sulfuric acid (50%) for 120 minutes to block diffusion of sodium ions from the glass support into the TiO₂ film during annealing process. which could affect crystallization of titania film and afterwards influence photocatalytic properties. After the boiling process the glass plates were rinsed with deionised water and dried.

3.2.2 Sol synthesis

Sol-gel method was used to prepare liquid media precursor of the titania studied layers. Sol with reverse micelle system in the experimental procedure was prepared using titanium(IV)isopropoxide TTIP as a precursor, nonionic surfactant Triton X 102 and cyclohexane as a solvent. Sol-gel process here stands for incomplete hydrolysis of a precursor and condensation of intermediates that run in the cores of reverse micelles of the surfactant.

The material printing was used as a deposition technique. The sol composition, mainly suitable solvent, occurred to be a fundamental issue, as solvents with high volatility cause a nozzle blockage. Reverse micelle sol optimization was studied at the Photochemical laboratory, Brno University of Technology by monitoring sol behavior during jet printing deposition. Xylene occurred to be a suitable solvent. A group of sols X, 2X, 3X and 4X, differing in the solvent ratio, was characterized by density and viscosity. The sol properties are included in Table 1.

Table 1 Composition and properties of prepared sols

Sol designation	X	2X	3X	4X
Xylene (ml)	5.1	10.2	15.3	20.4
Triton X 102 (ml)		2.5		
Demineralized water (ml)		0.06		
TTIP (ml)		1		

Automated Micro Viscometer AMVn combined with Density Meter DMA 4500 was used for measurement of dynamic viscosity. A solution is dosed into a glass capillary, which is place in the device under specified angle. A metal ball thrown into the capillary dives to the lower end of the capillary. On the way down the metal ball passes two sensors. Viscosity is calculated from the time period spent by the metal ball between those two sensors.

The measurement was kept at 25 °C. The size of the glass capillary and the metal ball were 1.6/1.5 mm, respectively. The slope of the capillary was 70 °. Dynamic viscosity was calculated as an average of four measurements.

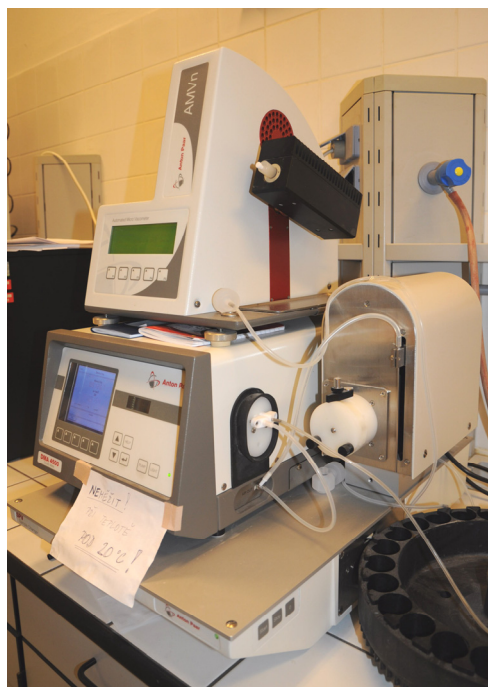


Figure 17 Automated Micro Viscometer AMVn combined with Density Meter DMA 4500

The process of sol optimization signed the sol composition 3X as the most suitable one for material printing deposition technique. The solution was prepared as follows: xylene (10.2 ml) was mixed with Triton X 102 (2.5 ml). After adding 0.06 ml of water by micropipette under stirring the solution became turbid and cleared up after 15 minutes of further vigorous stirring. In the end 1 ml of TTIP was added drop wise turning the sol orange-yellow. After centrifugation the sol was stored at 5 °C in a glass bottle wrapped in aluminum foil.

3.2.3 Deposition of layers

Thin layers of titanium dioxide were deposited by a specialized experimental inkjet printer FUJIFILM Dimatix (Figure 19). The prepared sol acts as ink in the ink tank. Before filling the sol into the ink tank the sol was sonicated for 5 minutes and filtered through a 0.2 μm membrane filter (Pall Corporation, USA). A Dimatix 10 pL printing head (containing 16 nozzles) was attached to the tank and mounted into the Dimatix printer. The nozzle temperature was 40 °C. The nozzle span was 20 μm, the nozzle shift was 4.5 °.

A printer settings optimization is very important to obtain satisfactory results. Viscosity is just one of few properties that predict the suitability of sol solution for inkjet printing deposition. Wetting ability of sol, which is generally low, needs to be mentioned as a relevant item in layer preparation. Wettability is closely associated with changing nozzle span. Too big nozzle span leads to a banding structure of layers but a fully coated surface is a desired image (Figure 18). Balance between the sol viscosity and nozzle span resulted in the sol 3X being the most suitable sol for material printing deposition technique.

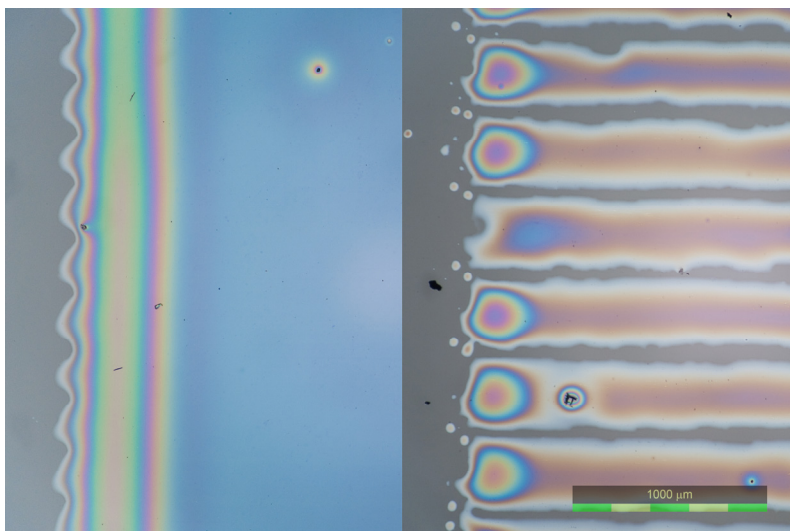


Figure 18 Wetting behavior of printed sols. Printing with suitable nozzle span (left) and too big nozzle span (right).

Optimized sol 3X was printed on the soda-lime glass support (50×50×1.1 mm, Merci, Czech Republic and 25×75×1.1 mm, Paul Marienfeld, Germany) by ink-jet printing. The glass supports of both sizes were first immersed into a solution of Triton X 102 in isopropyl alcohol of 1 vol. % and immediately dried in N₂ flow. This pretreatment ensures better and even wetting of the substrate by the printed sol.

Squared patterns (40×40 mm and 20×20 mm) were printed onto the above mentioned glass substrates, respectively. Printed layers were dried for 30 minutes at 110 °C. This step is marked as gelling step, when sol turns into gel. Calcination step at 450 °C for 4 hours followed to remove the organic content from the coatings. In this work films of 1, 2, 3 and 4 layers were prepared to obtain different thicknesses. For the multiple layers gelling step appeared after each layer deposition and the calcination step was performed after the very last gelling step.

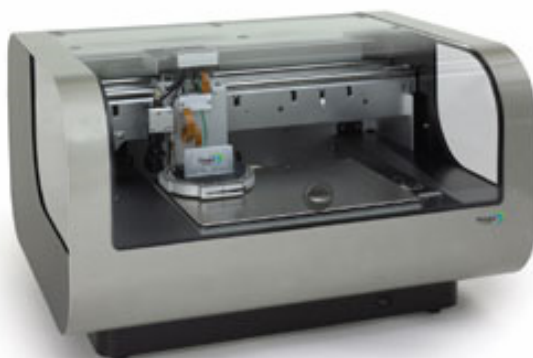


Figure 19 FUJIFILM Dimatix Materials Printer DMP-2800

3.3 Description of layers

3.3.1 Optical microscopy/Digital microphotography

The quality of prepared layers was investigated by optical microscope Nikon Eclipse E200. The records of prepared films of titanium dioxide of 1–4 layers were obtained from a digital camera Nikon D5000 mounted on the optical microscope. Reflected light microscopy was used to examine the prepared films. Microphotographs were obtained with 4×, 10× and 20× magnification.

3.3.2 Scanning electron microscopy

The surface topology was studied by SEM. Images were performed by the LabSensNano laboratory (The Faculty of Electrical Engineering and Communication, Brno University of Technology). Scanning electron microscope MIRA II LMU, Tescan, was used to record pictures of titanium dioxide films of 1–4 layers.

3.3.3 Photoinduced hydrophilicity

Photoinduced hydrophilicity (wettability) of TiO₂ coatings was expressed by contact angle as a function of irradiation time. The contact angle (CA) measurement was executed by Contact Angle System OCA 10, DataPhysics device (Figure 20). It requires manual sampling. The device obtains operating elements, which enables to place drops properly on the TiO₂ surface. It also provides drop visualization and subsequent picture storage due to the CCD camera and SCA software. The CA measurement can be taken in various periods of time after the drop is placed on the studied surface. The software enables to evaluate contact angle formed between the tangent of the drop profile and the base line of the surface.

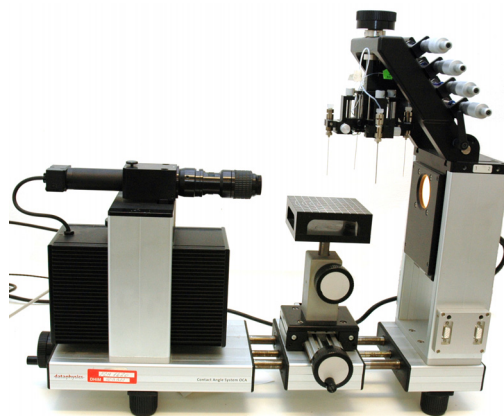


Figure 20 Contact Angle System OCA 10. DataPhysics device

The CA was measured on soda-lime glass supports with 1–4 coatings of titanium dioxide obtained by material printing. A drop of demineralized water of 10 μl was placed on the examined layer and after 5 s the contact angle was measured. The final value of CA was calculated as an average of five measurements from different parts of each layer.

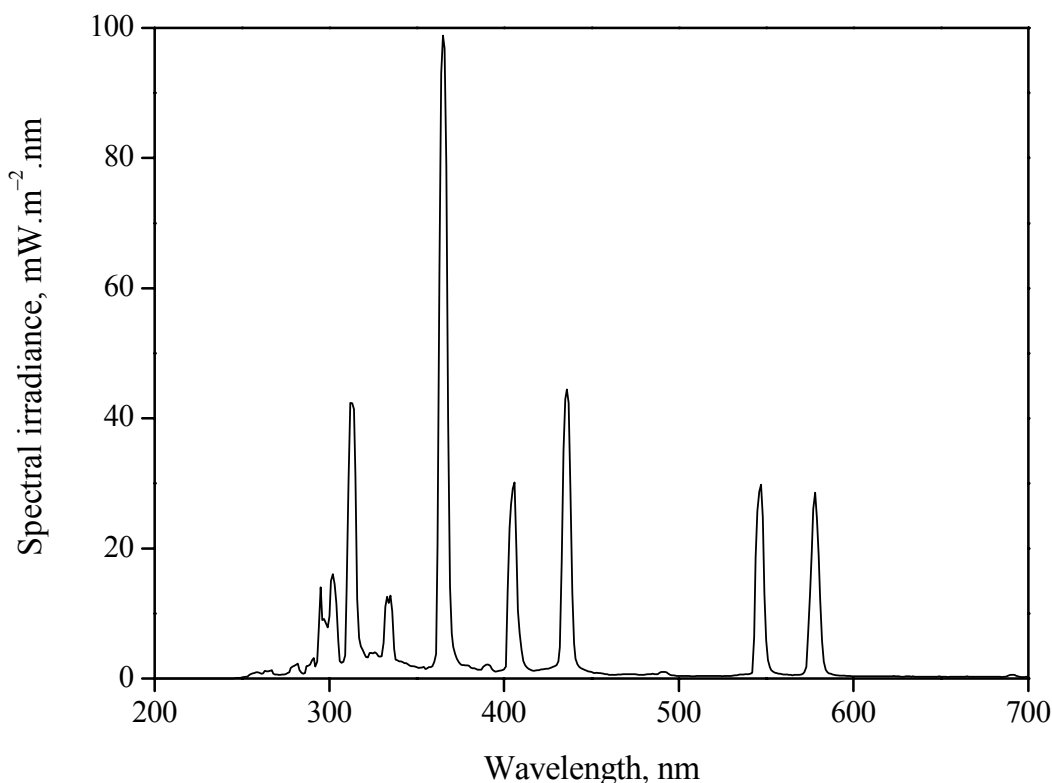


Figure 21 Emission spectrum of the Osram HQL 125 W lamp

Osram HQL 125 W lamp with irradiance of 2.1 mW.cm^{-2} was used as a light source; Figure 21 represents emission spectrum. Values of CA for each TiO_2 layer were obtained in 0, 1, 2, 7, 15 and 30 minutes of irradiation.

3.4 Photocatalytic experiments

3.4.1 Photocatalytic degradation of 2,6-dichloroindophenol

An ink indicator based on the redox dye 2,6-dichloroindophenol (DCIP) allows the rapid assessment of the activity of thin films. The oxidation reaction of DCIP occurs on the titanium dioxide surface under irradiation of suitable wavelength. Hydroxyl and superoxide radicals formed on the surface can attack molecules of DCIP. In the first step DCIP undergoes dechlorination reaction followed by oxidation of carbon-structure, resulting in carboxylic acids formation. Carboxylic acids undergo very fast decarboxylation.

Soda-lime glass plates ($50 \times 50 \times 1.1 \text{ mm}$) coated by 1–4 layers of TiO_2 by material printing on FUJIFILM Dimatix printer were used as samples. Each sample was first irradiated for 15 minutes under the light source of mentioned intensity to activate titania photocatalyst. The volume of DCIP was 50 cm^3 , the initial concentration of DCIP was $2.10^{-5} \text{ mol.dm}^{-3}$. Philips Metal-halide lamp HPA 400/30 SD was used as the UV light source; see Figure 22.

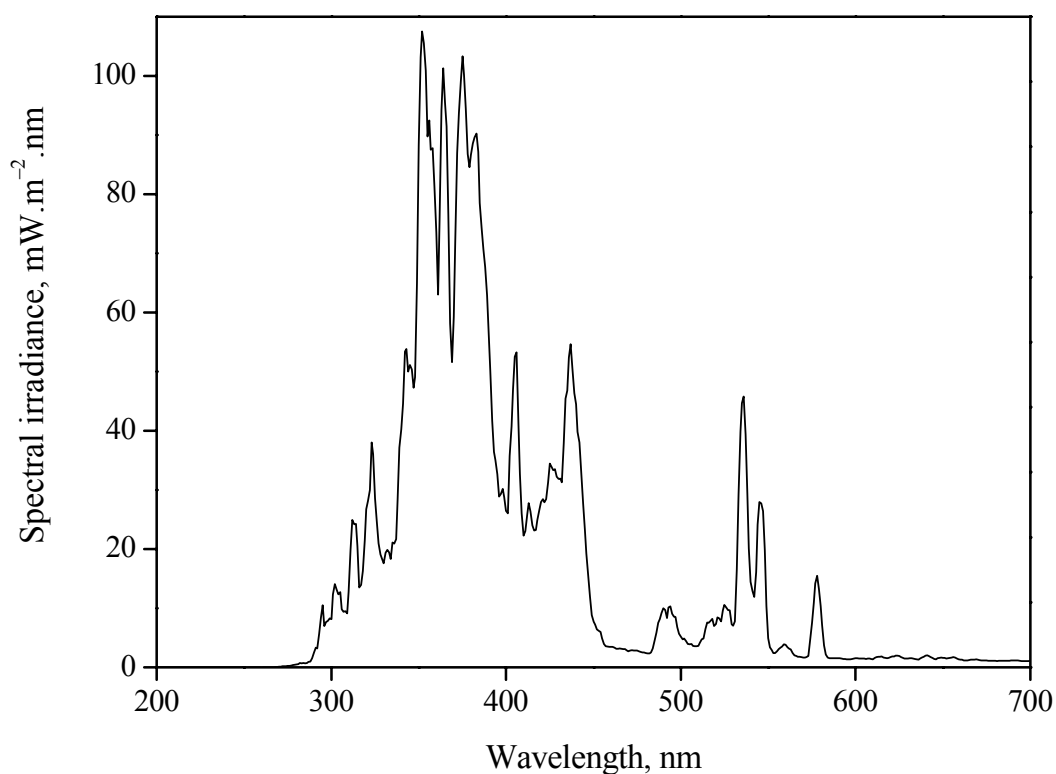


Figure 22 Emission spectrum of the metal-halide lamp Philips HPA 400/30 SD.

After that the sample was placed into a flow reactor on a rotary sample holder (Figure 23). The whole volume of DCIP solution was poured into the reactor. The reactor chamber was immediately covered by a transparent PE foil to prevent solution evaporation. Continuous flow of the model substance was maintained by a peristaltic pump. The surface of active titania layer was constantly watered from above. Due to the circular movement of the sample holder the model solution was easily spread over the whole deposited surface.

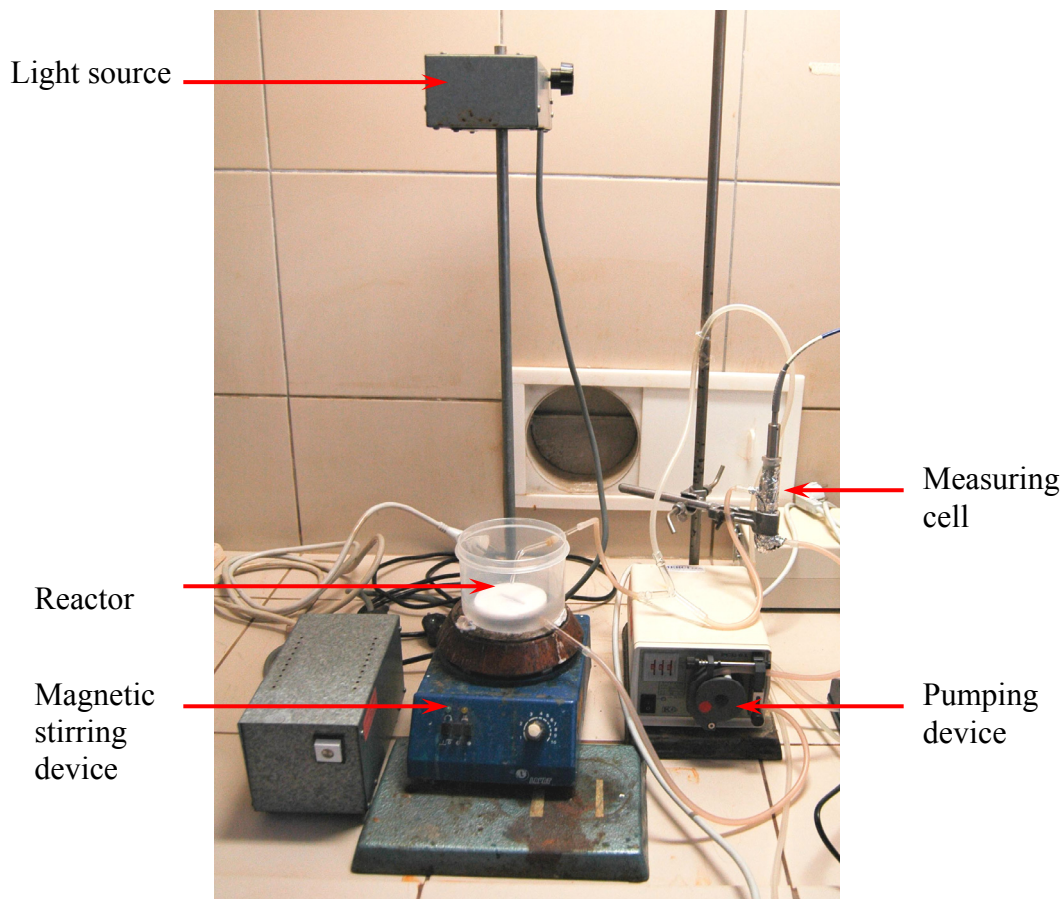


Figure 23 Arrangement of measuring system

The obtained rate of flow was $1.3 \text{ cm}^3 \cdot \text{s}^{-1}$ ($4.8 \text{ dm}^3 \cdot \text{hod}^{-1}$). The irradiation intensity of Philips light source, measured by Radiometer X 97, was set to $7.5 \text{ mW} \cdot \text{cm}^{-2}$ by the adjustment of the distance between the bulb and the surface of examined TiO_2 layer. Spectra Suite Ocean Optics software of fiber spectrometer provided on-line data collecting every 1 minute. Change of DCIP concentration proved by decrease in its absorption maximum at 600 nm was observed during the experiment as a result of the photocatalytic oxidation reaction. Each experiment ran for 40 minutes and was repeated three times. Reaction with a glass support without titanium dioxide layer represented a reference sample.

3.4.2 Photocatalytic degradation of stearic acid

3.4.2.1 Stearic acid deposition

Liquid media of stearic acid was deposited on previously prepared layers of titanium dioxide of 1–4 layers on soda lime glass supports ($25 \times 75 \times 1.1 \text{ mm}$). $0.1 \text{ mol} \cdot \text{dm}^{-3}$ solution of stearic acid (SA) in toluene was mixed with isobutyl alcohol in the ratio 1/9, respectively. Material printing by FUJIFILM Dimatix printer was used as a deposition technique. The temperature of a substrate placed in the printer was adjusted to $40 \text{ }^\circ\text{C}$. The higher temperature caused immediate evaporation of a solvent and fixation of SA on the substrate. Liquid media droplets of 10 pl were linearly spaced at $20 \text{ }\mu\text{m}$.

3.4.2.2 FT-IR spectrometry

Photocatalytic properties of prepared titania layers were studied by degradation of stearic acid (SA) carried out using infrared spectroscopy. FT-IR spectrometer Nicolet Impact 400 (Figure 24) was used as a measuring device to assess the level of SA present. Degradation reaction was estimated by a change of an integrated (peak) area under the FT-IR spectrum of SA as a function of exposure dose.



Figure 24 FT-IR spectrometer Nicolet Impact 400

Osram HQL 125 W lamp with intensity of $2.1 \text{ mW}\cdot\text{cm}^{-2}$ was used as an irradiation light source. The FT-IR absorption spectrum was measured periodically (every 10 minutes), as the irradiation proceeded. Values of peak area were calculated as an average of five measurements from different areas of the irradiated layers.

3.4.2.3 Contact angle measurement

Changes in contact angle were studied during the photocatalytic degradation of stearic acid. For device arrangement, see chapter 3.3.3. The CA was measured on soda-lime glass supports with 0–4 coatings of titanium dioxide obtained by piezoelectric deposition and one layer of stearic acid. The substrate without TiO_2 layers represents a blank (reference) sample for CA measurement of pure stearic acid degradation without influence of a photocatalyst. A drop of $10 \mu\text{l}$ was placed on the examined layer and after 5 s the contact angle was measured. The final value of CA was calculated as an average of five measurements from different parts of each layer.

Osram HQL 125 W lamp with intensity of $2.1 \text{ mW}\cdot\text{cm}^{-2}$ was used as a light source. Values of CA for each TiO_2 layer were obtained in 5-minute or longer intervals of irradiation.

3.5 Band gap determination

Band gap energies were calculated for prepared samples of titanium dioxide of 1–4 deposited layers. Band gap energies were estimated from reflectance curves of the layers. The measurement of reflectance spectra was realized in the darkness by Fiber Optic Spectrometer calibrated to a reflectance standard Labsphere. The spectrometer was equipped with a reflectance sensing head and a source of UV light. The sample response was measured under 45° .

4 RESULTS AND DISCUSSION

4.1 Dynamic viscosity determination

Dynamic viscosity was determined for series of sols described in Table 1 differing in the solvent content. The obtained values for X–4X are included in the Table 2. Increasing ratio of the solvent (xylene) resulted in the decreasing value of viscosity. The viscosity belongs to the most important properties to be balanced in sol preparation; solvent content in the sol influences strongly the process of sol deposition by material deposition technique.

Table 2 Determination of dynamic viscosity for sols with differing solvent ratio

Sol designation	X	2X	3X	4X
Density (g·cm ³)	0.94180	0.91270	0.90000	0.89250
Viscosity (mPa·s)	4.85650	2.03460	1.44140	1.17590
Viscosity standard deviation	0.00492	0.00333	0.00270	0.00015

4.2 Optical microscopy

The surface characteristic of TiO₂ films was described by optical microscopy. The views obtained are recorded as digital photographs, see Figure 25. The middle areas and the edges of the films were studied as different behavior over the deposited surface with variable number of coatings was expected.

There are no significant differences in the inner parts of the films for 1–3 layers. These layers provide smooth, well covered surface with no cracks or damages. The dots seen over the whole deposited area on all obtained images represent dust particles that were present on the glass plates during the sol deposition by material printing.

Small cracks start to appear on the edges with increasing number of layers. The edge parts of the three layered film even start to peel off. This behavior is much stronger for the film with four coatings (layers), where not only peeling off effect appears but also cracking over the coated area is observed. The highest number of coatings also means the highest film thickness and the highest tensile stress that the material is exposed to. Tensile stress caused by the organic matter of the layer plays important role when being pyrolyzed during the calcination step. The mass of the layer returns back to its original dimensions causing the layer cracking.

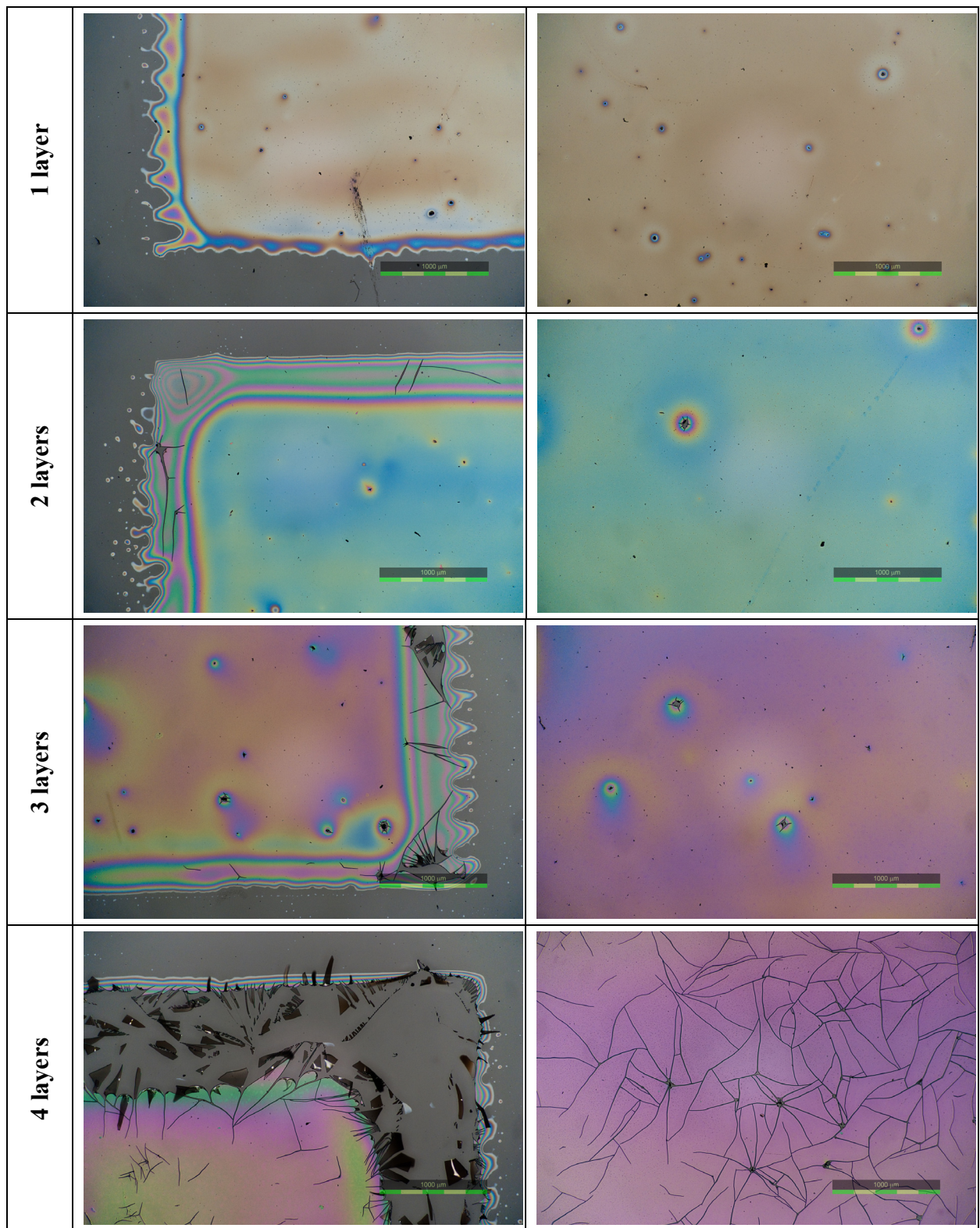


Figure 25 Microimages of TiO₂ films of 1–4 layers in polarized light: edges (left). the middle parts of the film (right)

4.3 Scanning electron microscopy

SEM images provide more detailed view on the prepared TiO_2 layers. The pictures on the Figure 26 show the film surface in nano-scale. There is no distinct difference between the SEM images for 1–4 layers. All the studied surfaces can be defined as similar layers with nano-cracks.

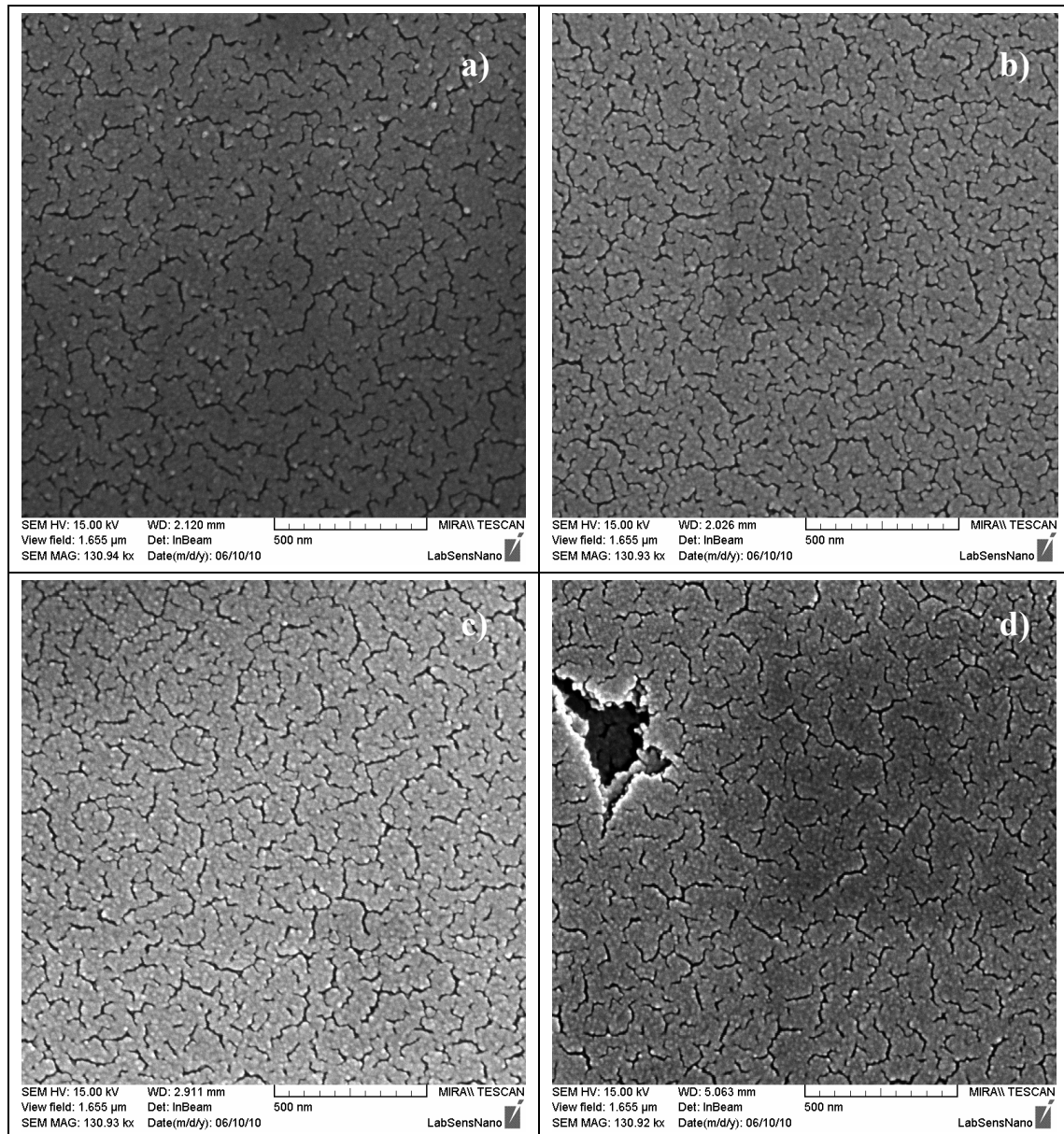


Figure 26 SEM images of TiO_2 films for 1–4 layers: a)–d) represent films of 1–4 layers, respectively

4.4 Band gap determination

Prepared layers were characterized by the band gap. Figure 32 shows results from reflectance measurement of titania films for 1–4 layers. The oscillation of the curves between 550 and 370 nm is due to the interference either between the film and the substrate (for one layer) or in addition between layers each other (multiple layers). Extrapolation of the reflectance versus wavelength curves results in the estimation of the band gap energy.

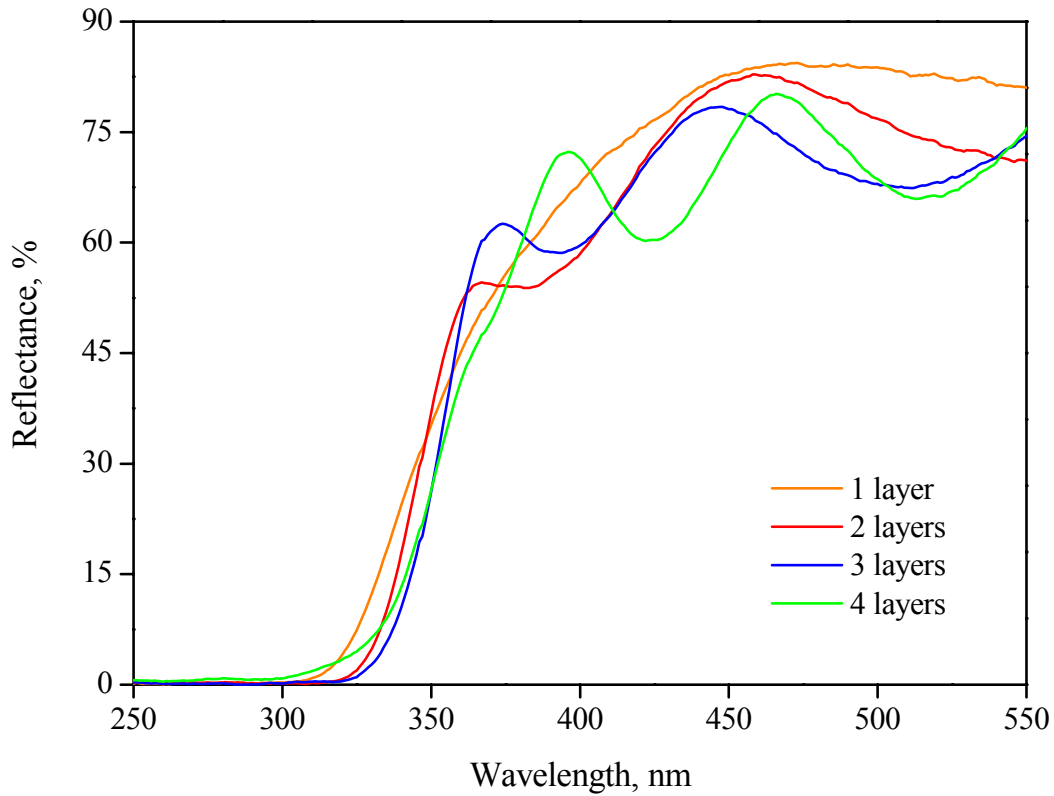


Figure 27 UV–VIS reflectance spectra of TiO_2 films for 1–4 layers

In this study the approach described in the chapter 2.10.3 was applied. Kubelka-Munk formalism was used to convert the reflectance into the equivalent absorption coefficient α_{KM} , according to the equation (19). After that the relations between the equivalent absorption coefficient α_{KM} for direct and indirect transition (equations (20) and (21)) and energy values were obtained (Figure 28). Extrapolation of the linear part of the curves to the x-axis brings the band gap value.

For more precise results the graphs were fitted by Boltzmann function in the specialized software Origin that provided parameters of the obtained function. The parameters were used in the equation (26) to calculate band gap energies for each layer. Obtained band gap energies for direct and indirect transitions are specified in Table 3 and Table 4.

$$E_{bg} = \left(-\frac{A_1}{2} - \frac{A_1 x_0}{4dx} \right) \cdot \frac{4dx}{-A_1} \quad (26)$$

The band gap value of 3.2 eV is ascribed in literature to the anatase form of titanium dioxide. In this study the obtained values of the direct transition model are closer to the 3.2 eV value. Due to this observation the prepared TiO₂ can be specified as the direct band gap semiconductor.

The Kubelka-Munk formalism used here is usually associated with powder form of semiconductors. This may be a reason why the obtained band gap energies of prepared TiO₂ are higher.

It can be also observed that the band gap energies for direct transition decrease with increasing number of deposited layers. This tendency is usually closely associated with the photocatalytic activity of prepared layers where the lower band gap energy results in higher rate constant of ongoing photocatalytic reaction.

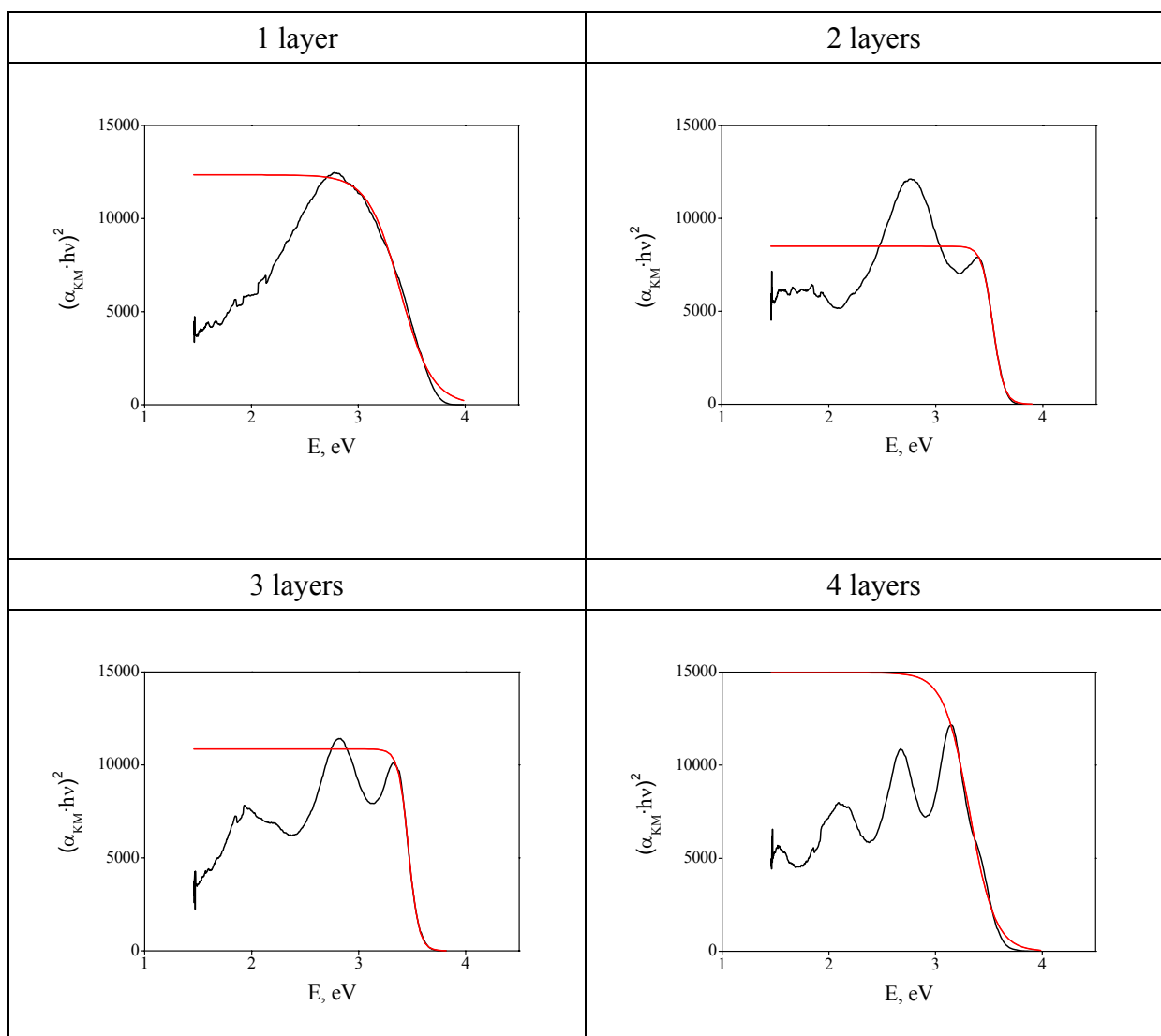


Figure 28 Absorption edge for direct transition in TiO₂ semiconductor: Boltzmann function fitting

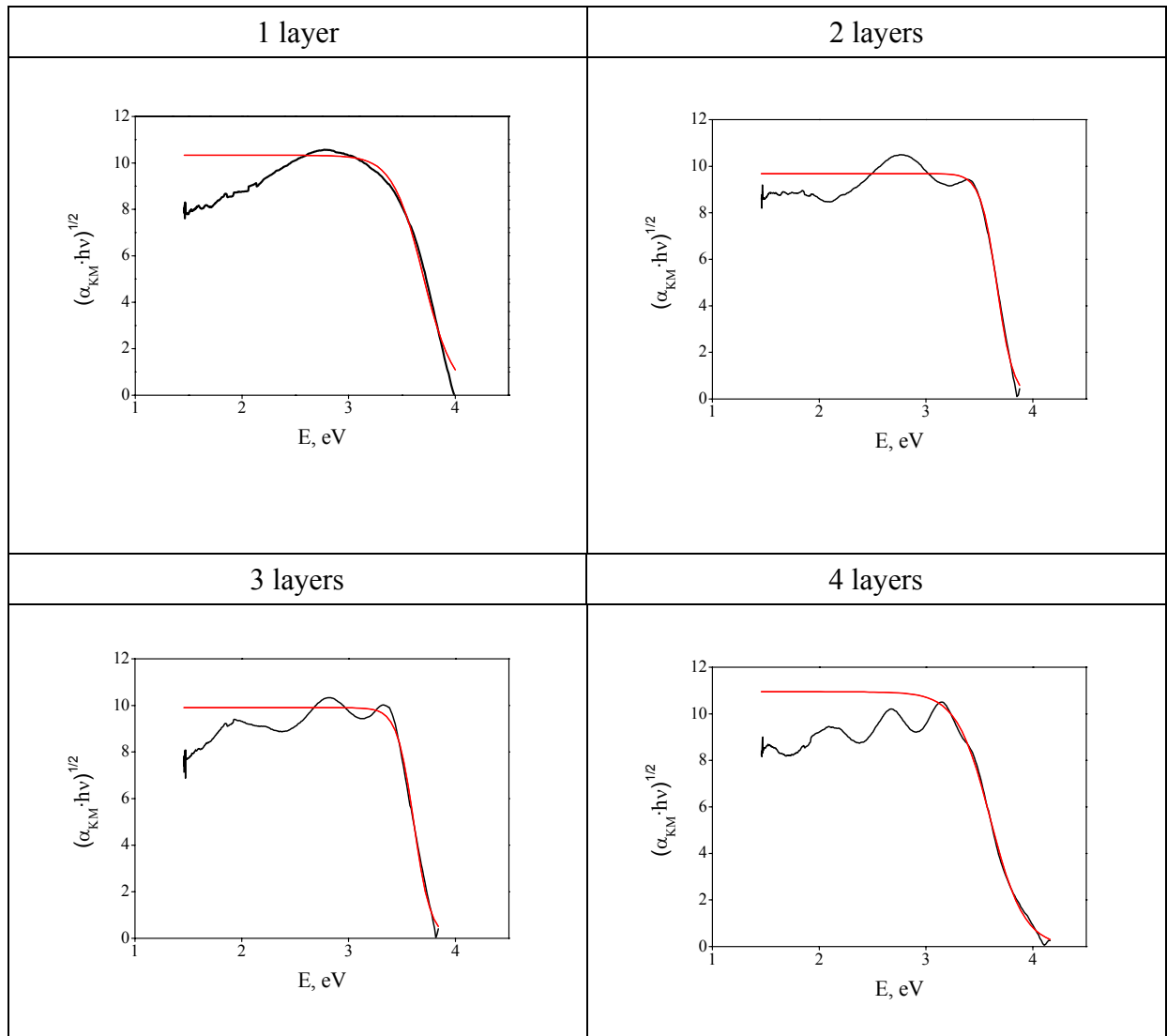


Figure 29 Absorption edge for indirect transition in TiO_2 semiconductor: Boltzmann function fitting

Table 3 Band gap energy for direct transition values for 1–4 layers of prepared TiO_2 films

Number of layers	Direct transition				E_{bg} (eV)	Absorption edge (nm)
	A_1	A_2	x_0	dx		
1	12344.1186	0.0000	3.3899	0.1499	3.6897	336
2	8498.6185	0.0000	3.5341	0.0510	3.6360	341
3	10851.7574	0.0000	3.4666	0.0471	3.5608	348
4	14967.8982	0.0000	3.3186	0.1191	3.5568	349

Table 4 Band gap energy values for indirect transition for 1–4 layers of prepared TiO₂ films

Indirect transition						
Number of layers	A_1	A_2	x_0	dx	E_{bg} (eV)	Absorption edge (nm)
1	10.3300	0.0000	3.6968	0.1422	3.9812	311
2	9.6840	0.0000	3.6638	0.0770	3.8178	325
3	9.9016	0.0000	3.6100	0.0789	3.7677	329
4	10.9454	0.0000	3.6025	0.1573	3.9172	317

4.5 Photoinduced hydrophilicity

Contact angle (CA) measurement was used as a method for describing photoinduced hydrophilicity (wettability) of TiO₂ coatings. The change of contact angle in time was recorded (Table 5) and calculated as the relation between relative contact angle and exposure dose (Figure 31). The prepared TiO₂ films with 1–4 layers were irradiated under the same conditions with irradiance of 2.1 mW·cm⁻².

Referred to the Figure 31 the kinetics of the CA decrease is the same. The layers behave different in the range of 2-15 minutes of irradiation where the one-layer film provides the fastest response in the CA decrease. At the end of irradiation the contact angle for all films is under 15°. According to the trend of the spectra it can be predicted that the CA under irradiation longer than 30 minutes will not decrease significantly furthermore.

Table 5 Absolute values of contact angles during irradiation of prepared TiO₂ films

Irradiation Time (min)	Contact angle (°)			
	1 layer	2 layers	3 layers	4 layers
0	43.1 ± 0.3	38.8 ± 0.7	38.2 ± 0.8	34.6 ± 0.3
1	29.9 ± 1.6	25.7 ± 0.6	28.6 ± 1.3	22.9 ± 0.6
2	21.8 ± 0.9	19.7 ± 0.5	20.9 ± 0.5	20.0 ± 0.8
7	16.8 ± 0.5	17.0 ± 0.1	17.1 ± 0.6	16.9 ± 0.5
15	14.1 ± 0.7	15.8 ± 0.8	15.4 ± 0.5	13.6 ± 0.3
30	13.5 ± 0.8	14.2 ± 0.4	11.8 ± 0.3	12.9 ± 0.6

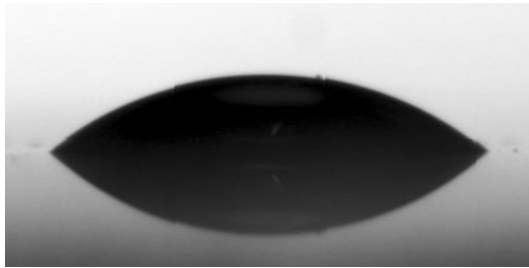
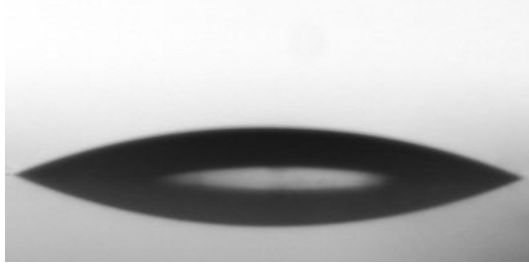
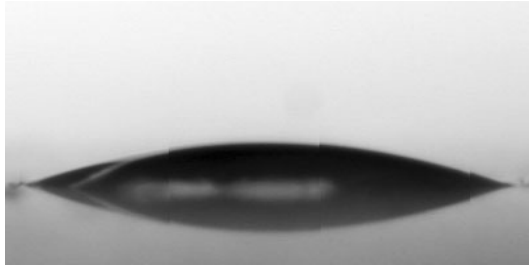
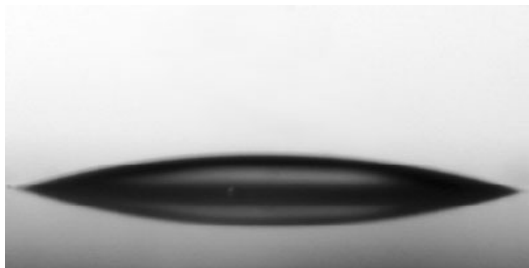

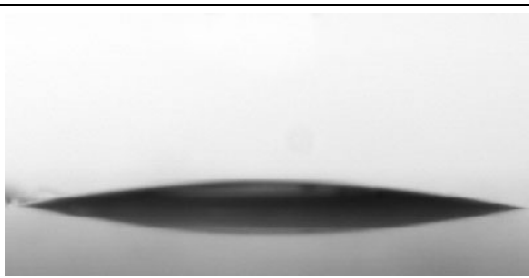
Irradiation time (min)	1 layer
0	
1	
2	
7	
15	
30	

Figure 30 Pictures of droplets on 1-layered TiO_2 film during irradiation for contact angles calculation

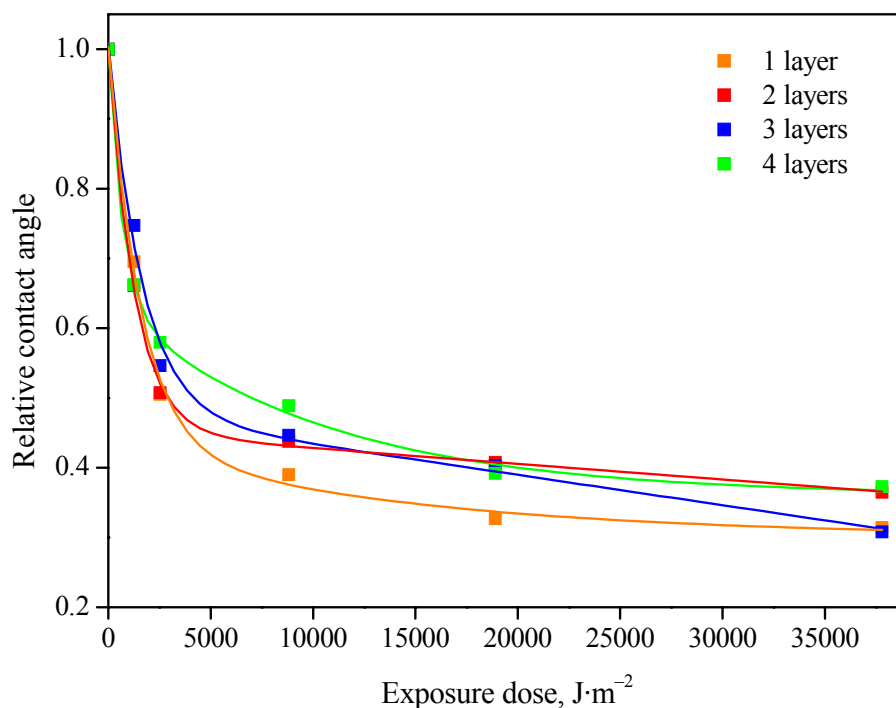


Figure 31 Contact angle measurement: Relative contact angle as a function of exposure dose

4.6 Photocatalytic activity of 2,6-dichloroindophenol

4.6.1 Calibration curve method

DCIP solutions of known concentrations were prepared to create a calibration curve for photocatalytic reaction of the model solution. Absorption characteristics in the range of wavelength 190–700 nm were measured. It was observed that the absorption maximum corresponds to 600 nm (Figure 32).

The calibration curve was obtained as a dependence of maximum absorbance on the molar concentration of the solution (Figure 33). The linear function was calculated as $y = 13790x$ with $R^2 = 0.992$.

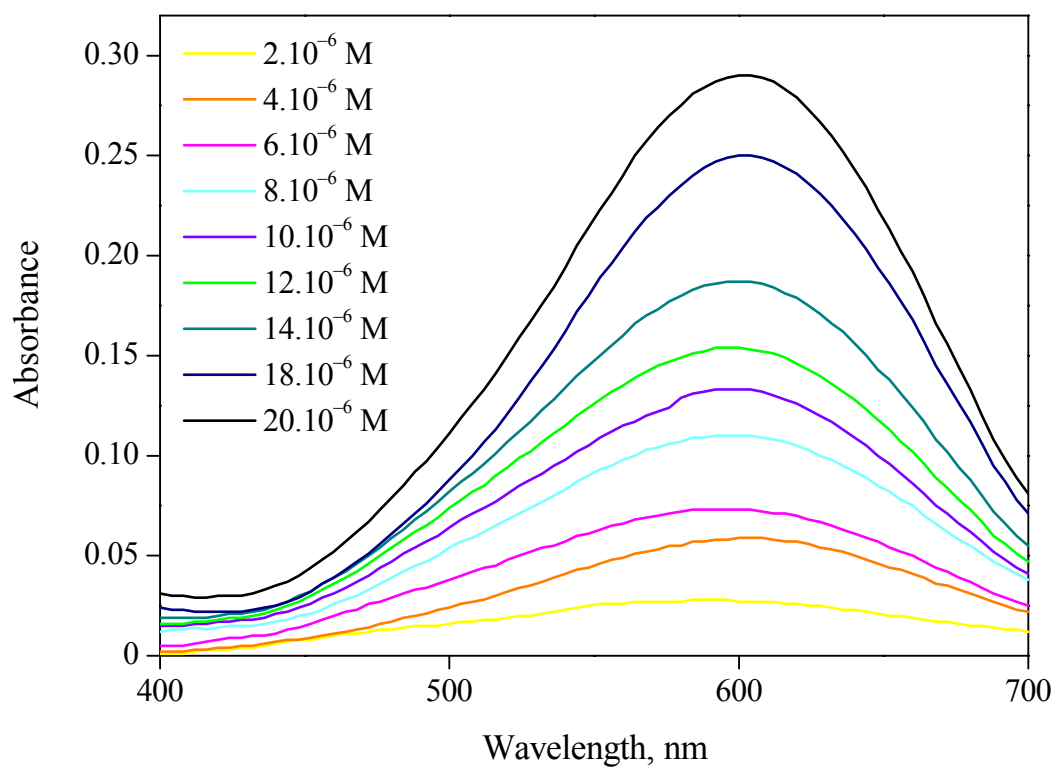


Figure 32 VIS absorption spectrum of 2,6-dichloroindophenol

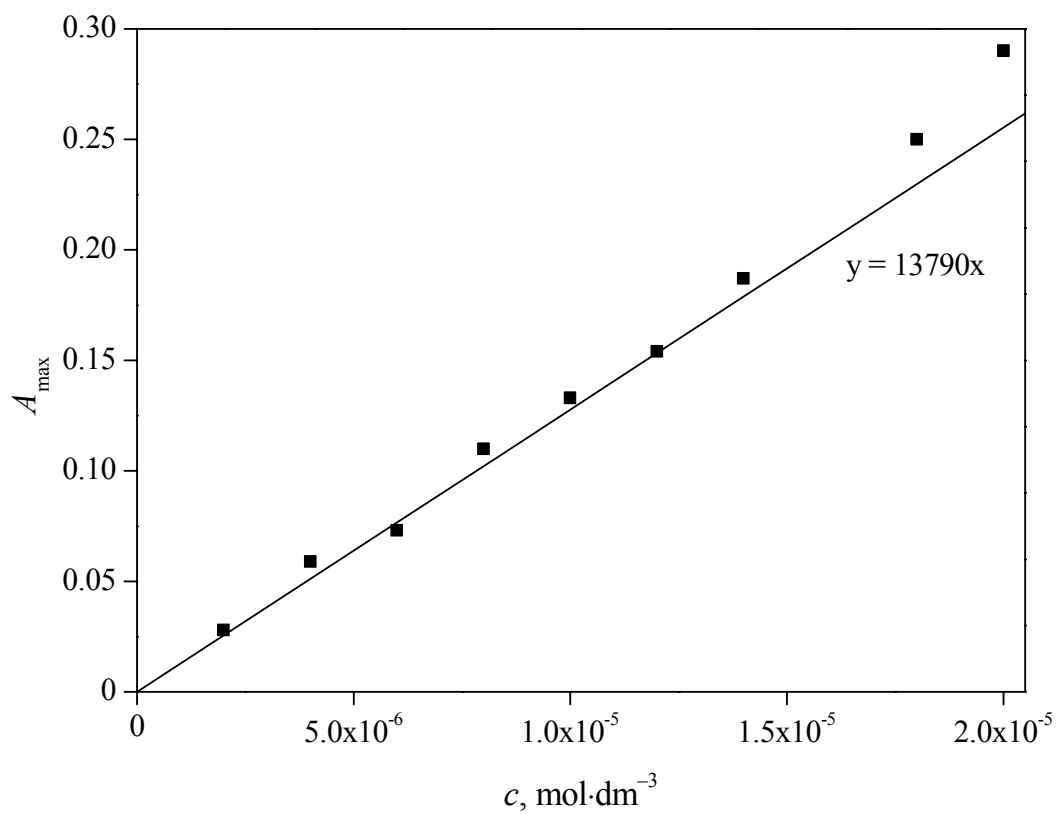


Figure 33 Calibration curve of 2,6-dichloroindophenol

4.6.2 Photochemical degradation of 2,6-dichloroindophenol

Absorption spectra of three-layered titania film during the photocatalytic reaction for 60 minutes under irradiance of $7.5 \text{ mW}\cdot\text{cm}^{-2}$ are illustrated in Figure 34. The curve maximum, assigned to 600 nm, shows a slight blue shift, which corresponds to the visual observations of the DCIP solution turning from blue to pink colour.

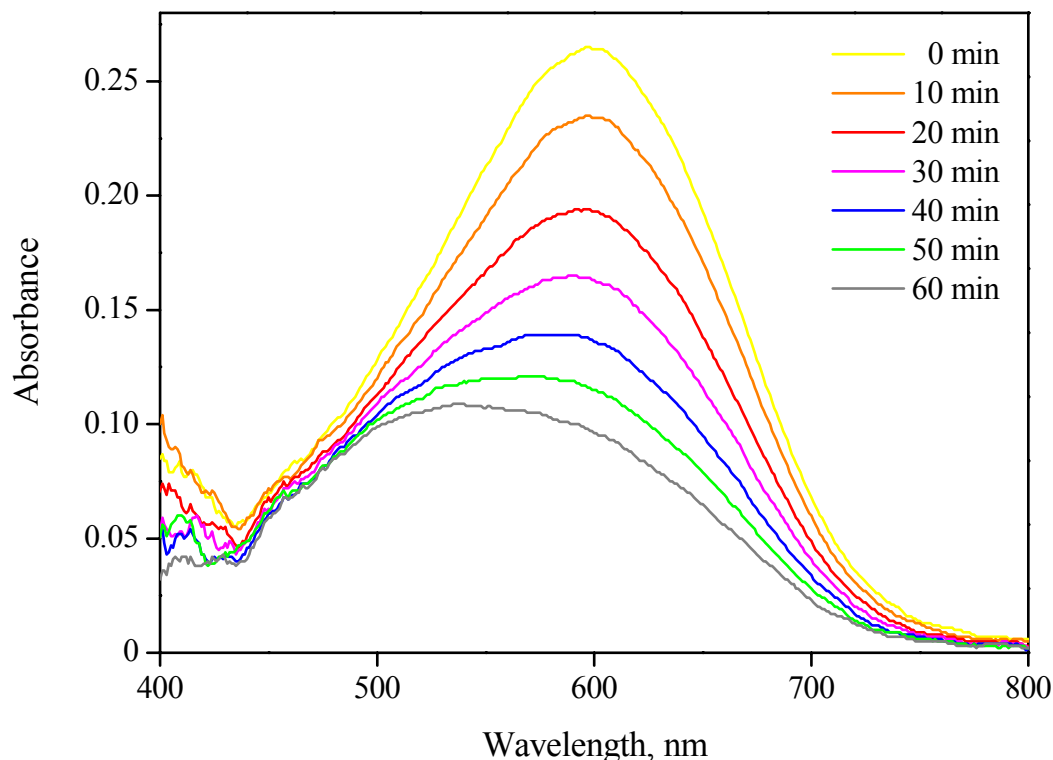


Figure 34 VIS absorption spectra of 2,6-dichloroindophenol photocatalytic oxidation reaction on the three-layered TiO_2 film.

It was observed that the photochemical degradation of 2,6-dichloroindophenol on the surface of titanium dioxide semiconductor can be described by the first order kinetics, see Figure 35 including average data of three measurements for each titania film. The oxidation reaction of the DCIP is much more complicated process than the first order reaction described by the equation (2). On the other hand the determination coefficient calculated for all studied layers was more than 0.99, which means that the selected reaction model was correct. The degradation reaction is then characterized by a formal rate constant. The photocatalytic reaction of DCIP for TiO_2 films with 1–4 layers is pictured in the Figure 36.

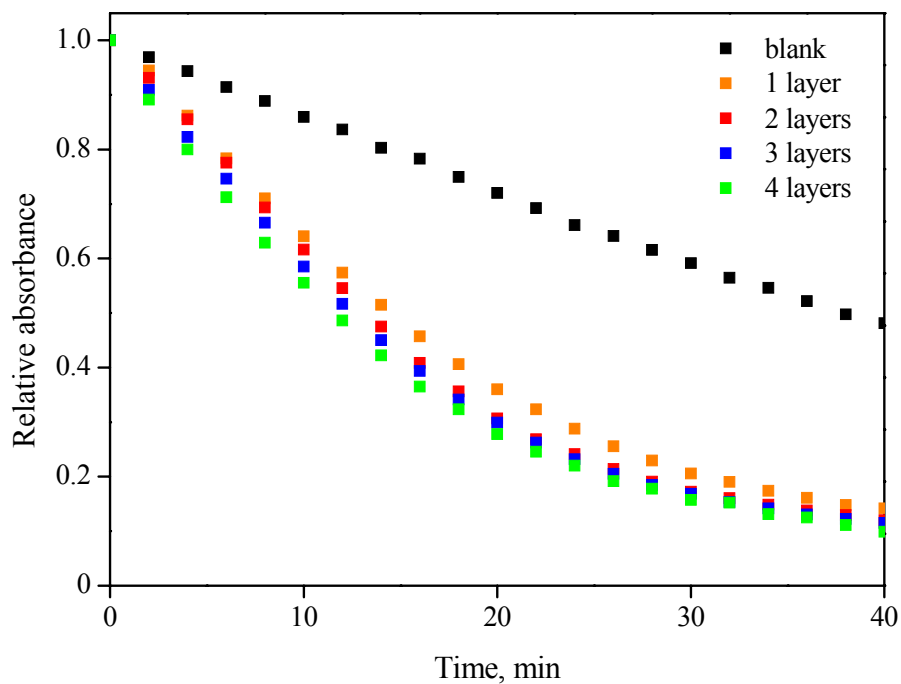


Figure 35 Degradation reaction of 2,6-dichloroindophenol on TiO_2 films with 1–4 layers: Relative absorbance as a function of time

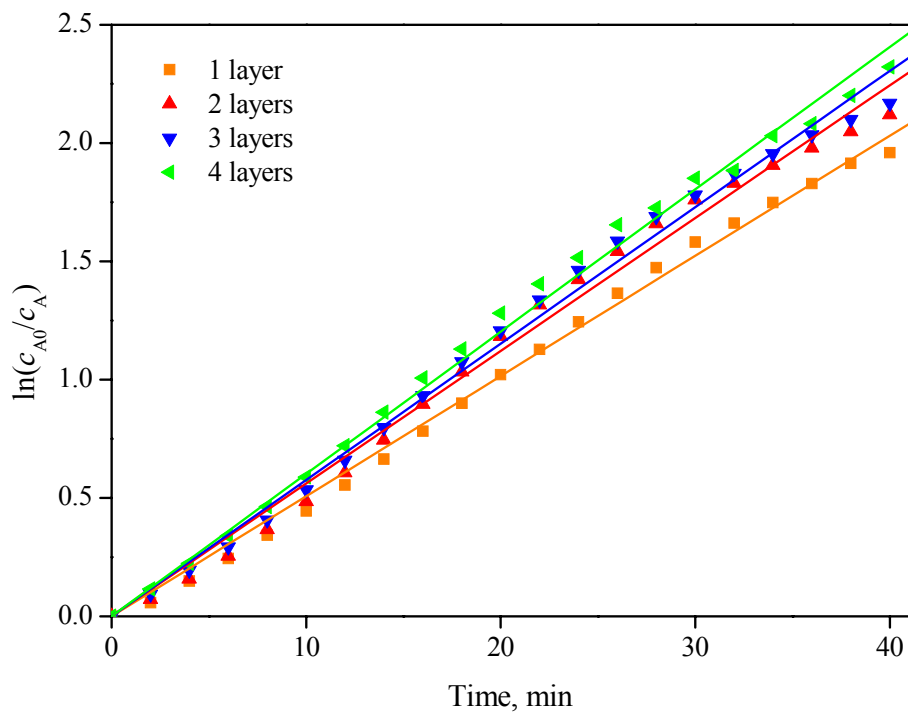


Figure 36 Degradation reaction of 2,6-dichloroindophenol: First order reaction on TiO_2 films with 1–4 layers

The rate constant was calculated according to the equation (27), where the rate constant is equal to the slope of the straight line.

$$\ln(c_{A0}/c_A) = f(t) \quad (27)$$

It was observed that not only photocatalytic degradation of DCIP on the TiO₂ surfaces with the rate constant \bar{k}_i as an average of three measurements occurred. Also direct degradation of the dye appeared under the set irradiation conditions. That is why the average rate constant \bar{k}_0 for the direct degradation out of three measurements was calculated. The rate constant k_0 describes a degradation reaction of the DCIP without any TiO₂ layer present in the reactor. The final formal rate constant was calculated as $(\bar{k}_i - \bar{k}_0)$ for each layer (Figure 37, Table 6). The standard deviation of the formal rate constants was calculated according to the equation (28).

$$\Delta(\bar{k}_i - \bar{k}_0) = (\bar{k}_i - \bar{k}_0) \sqrt{\left(\frac{\Delta\bar{k}_i}{\bar{k}_i}\right)^2 + \left(\frac{\Delta\bar{k}_0}{\bar{k}_0}\right)^2} \quad (28)$$

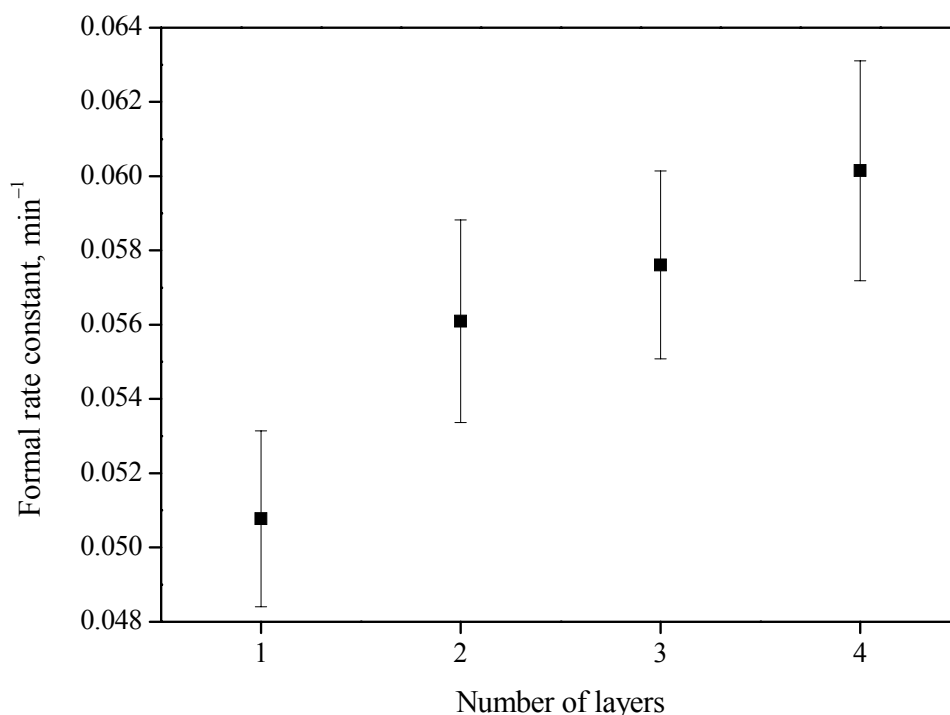


Figure 37 Degradation reaction of 2,6-dichloroindophenol: Formal rate constant as a function of number of TiO₂ layers

The formal rate constants of the photocatalytic reaction of DCIP on the active layers show that the efficiency of the reaction increases with the increasing number of layers under the specified conditions. This trend also corresponds to the discussion in the chapter 4.4, where the relation between increasing efficiency of TiO₂ by increasing number of active titania coatings was predicted by the band gap energy. The highest number of coatings resulted in the lowest band gap energy and the highest photocatalytic activity.

Table 6 Formal rate constants of 2,6-dichloroindophenol degradation reaction under irradiation of $7.5 \text{ mW}\cdot\text{cm}^{-2}$ calculated for 1–4 TiO_2 layers

Measurement	Rate constants (min^{-1})				
	k_0	k_1	k_2	k_3	k_4
1	0.01806	0.05053	0.05607	0.05668	0.05777
2	0.01633	0.05290	0.05827	0.05713	0.06208
3	0.01818	0.04890	0.05394	0.05903	0.06059
Average value \bar{k}_i	0.01752	0.05078	0.05609	0.05761	0.06015
Standard deviation $\Delta\bar{k}_i$	0.00104	0.00201	0.00217	0.00125	0.00219
Formal rate constant $(\bar{k}_i - \bar{k}_0)$	–	0.03325	0.03857	0.04009	0.04263
Standard deviation $\Delta(\bar{k}_i - \bar{k}_0)$	–	0.00237	0.00273	0.00253	0.00296

4.7 Photocatalytic activity of stearic acid

4.7.1 Photocatalytic degradation of stearic acid

FT-IR absorption spectra as a relation between absorbance and wavenumber during the SA decomposition reaction under irradiation of $2.1 \text{ mW}\cdot\text{cm}^{-2}$ for the range of $2600\text{--}3200 \text{ cm}^{-1}$ are shown in the Figure 38. Three peaks are observed: 2958 cm^{-1} , 2923 cm^{-1} and 2853 cm^{-1} , corresponding to the methyl and methylene groups of stearic acid, respectively.

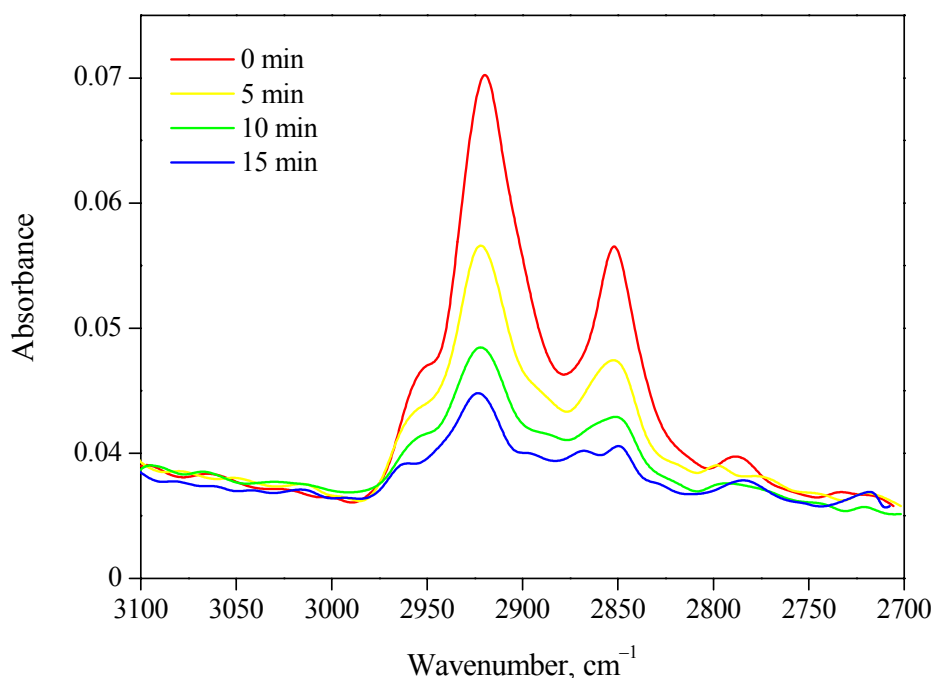


Figure 38 FT-IR absorption spectra of the film of stearic acid on the three-layered TiO_2 film recorded as a function of irradiation time

The maxima of peaks decrease within the stearic acid degradation reaction, resulting in the decrease of the integrated area under the absorption curve calculated for the wavenumber range of 2800–3000 cm^{-1} . The values of relative integrated areas (relative peak areas) during the SA degradation reaction on the prepared TiO_2 films of 1–4 layers as a function of exposure dose under $2.1 \text{ mW}\cdot\text{cm}^{-2}$ irradiation are specified in the Table 7. In the experiment, a stearic acid layer printed on a soda-lime glass support with no titanium dioxide layer, served as the blank sample. In the absence of a titania coating no change/decrease in the stearic acid FT-IR absorption spectrum over the irradiation period occurred.

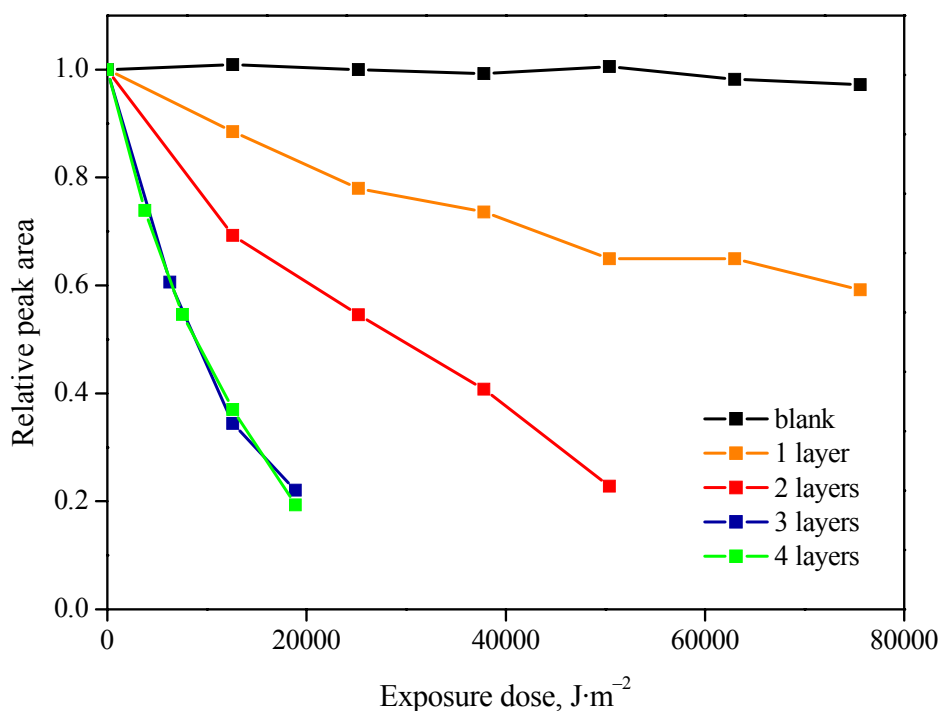


Figure 39 Degradation reaction of stearic acid: Relative peak area as a function of exposure dose under $2.1 \text{ mW}\cdot\text{cm}^{-2}$ irradiation

Referred to the Figure 39 the efficiency of the SA degradation increases with the number of printed layers of titania layers. The fastest decomposition of SA provides three- and four-coated TiO_2 films. There is no difference in the reaction time behaviour between these two films observed. For the conditions set for this particular experiment, the rate of SA decomposition reaction increases up to the three layers. For three and four layered films after 20 minutes of irradiation the amount of SA on the titania was so small that the peak area could not be calculated. The peak area for other films was measurable up to 40 minutes of irradiation.

Table 7 Relative peak area within the stearic acid degradation reaction

Irradiation time (min)	Exposure dose ($\text{J}\cdot\text{m}^{-2}$)	Relative peak area				
		blank	1 layer	2 layers	3 layers	4 layers
0	0	1.0000	1.0000	1.0000	1.0000	1.0000
3	3780	–	–	–	–	0.7389
5	6300	–	–	–	0.6061	–
6	7560	–	–	–	–	0.5462
10	12600	1.0089	0.8849	0.6929	0.3443	0.3702
15	18900	–	–	–	0.2204	0.1934
20	25200	1.0001	0.7801	0.5455	–	–
30	37800	0.9922	0.7362	0.4081	–	–
40	50400	1.0055	0.6492	0.2283	–	–
50	63000	0.9817	0.6495	–	–	–
60	75600	0.9723	0.5923	–	–	–

4.7.2 Contact angle measurement

As mentioned in the chapter 2.10.1.2 Evan et al. observed relation between photocatalytic activity and contact angle (CA) performance during the SA degradation reaction. This experiment was done also in this work where contact angle was measured during the SA degradation reaction. There was no change in CA for blank sample during the reaction. It was also assumed based on the obtained curves (Figure 40) that no relation between the rate of the CA decrease with the number of layers appeared, which does not correspond with the observations presented by Evan et al. in their study.

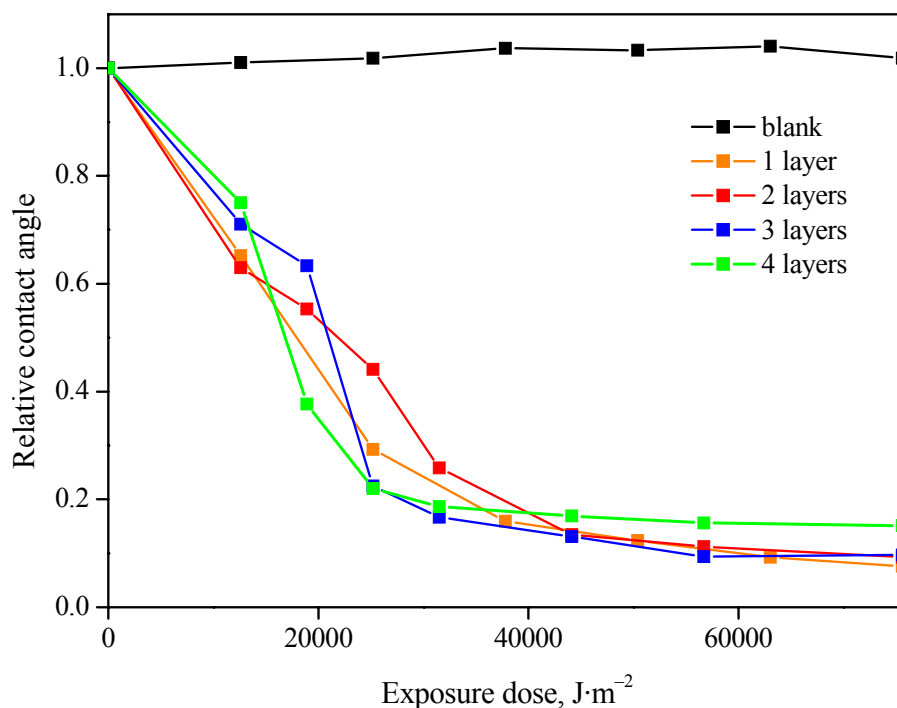


Figure 40 Contact angle measurement during the degradation reaction of stearic acid SA: Relative contact angle as a function of exposure dose

Table 8 Absolute contact angle values of water wetting during SA degradation reaction on 1–4 layered TiO₂ films

Irradiation Time (min)	Exposure dose (J·m ⁻²)	Contact angle (°)				
		blank	1 layer	2 layers	3 layers	4 layers
0	0	38.82 ± 0.38	97.82 ± 2.25	99.42 ± 1.55	80.84 ± 0.48	70.02 ± 2.36
5	12600	39.22 ± 1.01	63.80 ± 0.89	62.58 ± 1.65	57.44 ± 1.74	52.52 ± 1.11
10	18900	–	–	55.00 ± 0.95	51.22 ± 1.43	26.40 ± 2.52
20	25200	39.54 ± 1.10	28.68 ± 2.44	43.88 ± 0.66	18.20 ± 0.60	15.40 ± 0.28
30	31500	40.26 ± 1.43	15.62 ± 0.58	25.66 ± 1.52	13.48 ± 0.70	13.06 ± 0.35
40	44100	40.12 ± 0.80	12.12 ± 0.86	13.40 ± 1.13	10.58 ± 0.16	11.84 ± 0.21
50	56700	40.40 ± 1.47	9.08 ± 0.31	11.18 ± 0.37	7.58 ± 0.63	10.96 ± 0.39
60	75600	39.54 ± 0.74	7.44 ± 0.56	9.20 ± 0.70	7.82 ± 0.54	10.60 ± 0.48

All the prepared films behaved as hydrophilic surfaces at the end of the reaction. The CA values for all prepared films reached the border of 10° or lower at the end of the SA degradation reaction. The initial CA value decreased with increasing number of titania coatings. Values of absolute CA values are summarized in the Table 8.

5 CONCLUSION

- Thin transparent films of titanium dioxide with 1, 2, 3 and 4 layers were prepared by material printing technique. Soda-lime glass was used as a support for prepared films. Each glass support was treated by boiling in sulphuric acid to disable the sodium ions transfer from glass bulk to the prepared titania layer during the calcination process.
- Sol-gel process with reversed micelles was used as the preparation method of titanium dioxide semiconductor. The balance of sol components was discussed as the sol composition represents one of the most important conditions ensuring a suitable and smooth deposition process. Prepared sols of reverse micelles X–4X differing in the amount of solvent were described by density and dynamic viscosity. Non-ionic surfactant was used as a templating agent.
- Structure of surfaces of the prepared titanium dioxide films were studied by optical microscopy and scanning electron microscopy. According to the obtained microphotographs the prepared films of 1–3 layers show very similar surface structure with no cracking. Significant cracks are observed over the whole surface and edges of 4-layered TiO₂ film. SEM images verified the same nano-structure of all prepared films with small cracking over the mass of the semiconductor layers.
- Oxidation reaction of 2,6-dichloroindophenol and degradation reaction of stearic acid described the photocatalytic activity of prepared layers of titanium dioxide. Formal first order rate constant was calculated to determine the effectiveness of the oxidation reaction of DCIP. The rate constant increased with increasing number of coatings. Stearic acid (SA) degradation reactions confirmed similar behavior of prepared films. The stearic acid reaction occurred to be a simple method for verification of active titania surfaces.
- It was also observed that the photoinduced hydrophilicity is essentially associated with the photocatalytic ability of TiO₂ films. The hydrophilicity was expressed by contact angle CA that decreased by increasing exposure dose under defined irradiation. The kinetics of the CA change as a function of exposure dose were similar for all films. The decrease of CA to less than 40 % of the initial value confirms the photoinduced hydrophilicity of the studied films. The contact angle measurement was also used to describe lowering content of SA on the titania films during the SA degradation reaction verifying the photocatalytic properties of the examined films. The contact angle measurement within the SA degradation reaction verified photocatalytic properties of the prepared layers as the CA decreased as a result of SA degradation.

6 REFERENCES

- 1 ARPI, Majumder , et al. Study of gradual variation of structural, surface. *Journal of Physics: Conference Series* [online]. 2008, 012006, 100, [cit. 2011-04-22]. Dostupný z WWW: <http://iopscience.iop.org/1742-6596/100/1/012006/pdf/jpconf8_100_012006.pdf>.
- 2 LITTER, M. I.: Heterogenous photocatalysis. Transition metal ions in photocatalytic systems, *Applied Catalysis B: Enviromental*, 1999, vol. 23, p. 89–114.
- 3 BARTHELMY, David. *Mineralogy Database* [online]. 1997-2009 [cit. 2009-05-13]. Dostupný z WWW: <<http://www.webmineral.com/data/Rutile.shtml>>.
- 4 REYES-CORONADO, D , et al. Phase-pure TiO₂ nanoparticles: anatase, brookite and rutile . *Nanotechnology*. 5 March 2008, 19, 14, s. 1-10. Dostupný také z WWW: <<http://iopscience.iop.org/0957-4484/19/14/145605/cites>>.
- 5 TOMA, Filofteia-Laura, et al. Development of Photocatalytic Active TiO₂ Surfaces by Thermal Spraying of Nanopowders. *Journal of Nanomaterials*. 2008, no. 2008, s. 8.
- 6 MILLS, Andrew, et al. A Rapid Method of Assessing the Photocatalytic Activity of Thin TiO₂ Films Using an Ink Based on the Redox Dye 2,6-Dichloroindophenol. *International Journal of Photoenergy*. 2008, no. 2008, s. 6.
- 7 MILLS, Andrew , WANG, Jishun , MCGRADY, Mark . Method of Rapid Assessment of Photocatalytic Activities of Self-Cleaning Films. *J. Phys. Chem. B*. 2006, no. 110, s. 18324-18331.
- 8 FUJISHIMA, Akira, HASHIMOTO, Kazuhito, WATANABE, Toshiya. *TiO₂ photocatalysis : Fundamentals and Applications*. [s.l.] : [s.n.], 1999. 176 s. ISBN 4-939051-03-X.
- 9 BARTOVSKÁ Lidmila: *Chemická kinetika* [online]. Version 1.0. Praha : VŠCHT Praha, 2008 [cit. 2009-05-13]. Available from www: <http://vydavatelstvi.vscht.cz/knihy/uid_isbn-978-80-7080-670-8/pages-img/obalka-1.html>. ISBN 978-80-7080-670-8.
- 10 KUMAR, K. Vasanth, PORKODI, K. , ROCHA, F. Langmuir–Hinshelwood kinetics – A theoretical study. *Catalysis Communications*. 2009, no. 9, s. 82-84.
- 11 LUND, Carl. *Su28_reading.pdf (application/pdf objekt)* [online]. 2005 [cit. 2009-05-13]. Dostupný z WWW: <http://www.eng.buffalo.edu/Courses/obsolete/ce429/study_units/readings/su28_reading.pdf>.

- 12 *Sol Gel Technology* [online]. 1998 [cit. 2009-05-13]. Dostupný z WWW: <<http://www.chemat.com/html/solgel.html>>.
- 13 *UBCerem* [online]. 2005 [cit. 2009-05-13]. Dostupný z WWW: <<http://www.ceramics.mmat.ubc.ca/introduction.html>>.
- 14 DRBOHLAVOVÁ, J.: Příprava fotokatalyticky aktivních povrchů, Brno, 2008. Disertační práce na Vysokém Učení Technickém v Brně na Ústavu fyzikální a spotřební chemie. Vedoucí diplomové práce Doc. Ing. Michal Veselý, CSc.
- 15 GUO, Bing , et al. Photocatalytic effect of the sol-gel derived nanoporous TiO₂ transparent thin films. *Thin Solid Films*. 2005, no. 479, s. 310-315.
- 16 KHATAEE, A. R. ; ALEBOYEH, H. ; ALEBOYEH, A. . Crystallite phase-controlled preparation, characterisation and photocatalytic properties of titanium dioxide nanoparticles. *Journal of Experimental Nanoscience* [online]. 2009, Volume 4, Issue 2, [cit. 2011-04-22]. Dostupný z WWW: <<http://www.informaworld.com/smpp/content~content=a911663390>>.
- 17 KRATZAT , Krystyna. *Encyclopedia of Surface and Colloid Science: Second Edition* [online]. Second edition. [s.l.] : Taylor & Francis , 04 January 2011 [cit. 2011-04-22]. Dostupné z WWW: <<http://www.informaworld.com/smpp/title~content=t713172975~link=cover>>. ISBN 978-0-8493-9614-4.
- 18 Chen, X.; Mao, S. S.: Titanium dioxide nanomaterials: synthesis, properties, modifications, and applications, *Chem. Rev.*, 2007, vol. 107, p. 2891–2959.
- 19 LIM, L.L.P.; LYNCH, R.J.; IN, S.-I. Comparison of simple and economical photocatalyst immobilisation procedures. *Applied Catalysis A: General*. 2009, 365, s. 214-221.
- 20 LITTER, Marta I. . Heterogeneous photocatalysis Transition metal ions in photocatalytic systems. *Applied Catalysis B: Environmental*. 1999, no. 23, s. 89-114.
- 21 BRINKER, C. Jeffrey; HURD, Alan J. Fundamentals of sol-gel dip-coating. *J. Phys. III France* [online]. 1994, 4, [cit. 2011-04-27]. Dostupný z WWW: <<http://hal.archives-ouvertes.fr/docs/00/24/91/79/PDF/ajp-jp3v4p1231.pdf>>.
- 22 *Group for Characterization and Development of Materials for Photonics and Optoelectronics - CSMFO Group* [online]. 2011, 24 March 2011 [cit. 2011-04-27]. Dip-coating. Dostupné z WWW: <<http://www.science.unitn.it/~gcsmf/facilities/dip-coating.htm>>.

- 23 *W_{www.brewerscience.com}* [online]. 2011 [cit. 2011-04-27]. Spin Coater Theory Brewer Science. Dostupné z WWW: <<http://www.brewerscience.com/research/processing-theory/spin-coater-theory>>.
- 24 HAKOLA, Liisa . Inkjet Printing For Making Fine Conductors and Multi Layer Electronics. In *UV & EB Technology Expo & Conference*. [s.l.] : [s.n.], 2006. s. 19. Dostupný z WWW: <http://www.vtt.fi/inf/julkaisut/muut/2006/RT2006_Hakola.pdf>.
- 25 VEILLET, Ray . *PicoJet | Technology - Drop-on-Demand IJ Printing* [online]. 2008 [cit. 2009-05-13]. Dostupný z WWW: <<http://www.picojet.com/drop-on-demand.asp>>.
- 26 LE, Hue P. . Progress and Trends in Ink-jet Printing Technology. *Journal of Imaging Science and Technology* [online]. 1998, no. 42 [cit. 2009-05-13]. Dostupný z WWW: <<http://www.imaging.org/resources/leinkjet/part2.cfm>>.
- 27 *HowStuffWorks* \ "How Inkjet Printers Work" [online]. 1998-2009 [cit. 2009-05-13]. Dostupný z WWW: <<http://computer.howstuffworks.com/inkjet-printer3.htm>>.
- 28 DZIK, Petr; VESELÝ, Michal. Uživatelské zkušenosti s materiálovou tiskárnou Fujifilm Dimatix. In *POLYGRAFIA ACADEMICA 2010 : seminár so zahraničnou účasťou*. Bratislava : Nakladateľstvo STU v Bratislave, 2010. s. 107-114. ISBN 978-80-227-3340-3.
- 29 *W_{www.dimatix.com}* [online]. 2011 [cit. 2011-05-10]. Dimatix Materials Printer DMP-2800 - FUJIFILM Dimatix. Dostupné z WWW: <http://www.dimatix.com/divisions/materials-deposition-division/printer_cartridge.asp>. Konec formuláre
- 30 NARAYANASWAMY, Arun , et al. Synthesis and characterization of porous TiO₂ with wormhole-like framework structure. *J Porous Mater.* 2008, no. 15, s. 21-27.
- 31 KUZNETSOVA, I.N.; BLASKOV, V.; ZNAIDI, L. Study on the influence of heat treatment on the crystallographic phases of nanostructured TiO₂ films. *Materials Science and Engineering: B* [online]. 2006, 137, 1-3, [cit. 2011-04-23]. Dostupný z WWW: <http://www.sciencedirect.com/science?_ob=ArticleURL&_udi=B6TXF-4MD9G81-2&_user=10&_coverDate=02%2F25%2F2007&_rdoc=1&_fmt=high&_orig=gateway&_origin=gateway&_sort=d&_docanchor=&view=c&_searchStrId=1728090431&_rerunOrigin=google&_acct=C000050221&_version=1&_urlVersion=0&_userid=10&md5=9c879d76c8a73fc22cb89e148ee3481d&searchtype=a>.
- 32 AN, Taicheng, et al. Structural and photocatalytic degradation characteristics of hydrothermally treated mesoporous TiO₂. *Applied Catalysis A: General*. 30 November 2008, Volume 350, Issue 2, s. 237-243.

- 33 ARCONADA, N., et al. Synthesis and photocatalytic properties of dense and porous TiO₂-anatase thin films prepared by sol-gel . *Applied Catalysis B: Environmental*. 2 February 2009, Volume 86, Issue 1-2, s. 1-7.
- 34 MOROZOVA, M., et al. Role of the template molecular structure on the photoelectrochemical functionality of the sol-gel titania thin films. *J Sol-Gel Sci Technol*. 6 July 2009, 52, s. 398-407.
- 35 WATANABE, Toshiya, et al. Photocatalytic Activity and Photo-Induced Wettability Conversion of TiO₂ Thin Film Prepared by Sol-Gel Process on a Soda-Lime Glass. *Journal of Sol-Gel Science and Technology*. 2000, no. 19, s. 71-76.
- 36 CHOMOUCKÁ, J.: *Příprava samočisticích fotokatalyticky aktivních vrstev*, Brno, 2005. Diplomová práce na Vysokém Učení Technickém v Brně na Ústavu fyzikální a spotřební chemie. Vedoucí diplomové práce Doc. Ing. Michal Veselý, CSc.
- 37 MILLS, Andrew; MCFARLANE, Michael. Current and possible future methods of assessing the activities of photocatalyst films. *Catalysis Today*. 2007, 129, s. 22-28.
- 38 BREZOVÁ, V., a kol. Photocatalytic oxidation of 2,6-dichloroindophenol in the titanium dioxide aqueous suspension. *Chemical Papers*. 1991, vol. 45, s. 233-246.
- 39 *KSV Instruments Ltd: Contact Angle* [online]. 2009 [cit. 2009-05-13]. Dostupný z WWW: <<http://www.ksvltd.com/content/index/keyca>>.
- 40 Bartovská Lidmila, Šišková Marie: *Fyzikální chemie povrchů a koloidních soustav* [online]. Version 1.0. Praha : VŠCHT Praha, 2005 [cit. 2011-04-23]. P. 025. Available from www: <http://vydavatelstvi.vscht.cz/knihy/uid_isbn-80-7080-579-X/pages-img/025.html>. ISBN 80-7080-579-X
- 41 *Dissemination of IT for the Promotion of Materials Science (DoITPoMS)* [online]. University of Cambridge : November 2007 [cit. 2011-04-26]. DoITPoMS TLP - Introduction to Semiconductors - Direct and Indirect Band Gap Semiconductors. Dostupné z WWW: <<http://www.doitpoms.ac.uk/tlplib/semiconductors/direct.php>>.
- 42 VAN ZEGHBROECK, B. *Colorado.edu* [online]. 2007 [cit. 2011-04-26]. Optoelectronic devices. Dostupné z WWW: <http://ecee.colorado.edu/~bart/book/book/chapter4/ch4_6.htm#fig4_6_2>.
- 43 HOPKINS, Simon. *Department of Materials Science & Metallurgy, University of Cambridge* [online]. University of Cambridge : 2011 [cit. 2011-04-27]. Applied Superconductivity and Cryoscience Group - Characterisation - UV-vis spectroscopy. Dostupné z WWW: <<http://www.msm.cam.ac.uk/ascg/characterisation/uvvis.php>>.

- ⁴⁴ www.siliconfareast.com [online]. 2005, 2005 [cit. 2011-05-10]. Optical Microscopy. Dostupné z WWW: <<http://www.siliconfareast.com/optical.htm>>.
- ⁴⁵ DAVIDSON , Michael W. Molecular Expressions Microscopy Primer Specialized Microscopy Techniques [online]. 2010 [cit. 2011-05-10]. Dostupné z WWW: <<http://micro.magnet.fsu.edu/primer/techniques/index.html>>.
- ⁴⁶ DAVIDSON, Michael W.; ABRAMOWITZ, Mortimer. [Http://microscopy.fsu.edu](http://microscopy.fsu.edu) [online]. National High Magnetic Field Laboratory, Florida : 2005 [cit. 2011-05-10]. OPTICAL MICROSCOPY. Dostupné z WWW: <<http://micro.magnet.fsu.edu/primer/pdfs/microscopy.pdf>>.
- ⁴⁷ [Http://lms.vscht.cz](http://lms.vscht.cz) [online]. 2003 [cit. 2011-05-10]. Infračervená spektroskopie a její techniky. Dostupné z WWW: <<http://lms.vscht.cz/Zverze/Infrared.htm#Techniky>>.
- ⁴⁸ www.newport.com [online]. Irvine CA, USA : Newport corporation, 2011 [cit. 2011-05-10]. Introduction to FT-IR Spectroscopy. Dostupné z WWW: <<http://www.newport.com/Introduction-to-FT-IR-spectroscopy/405840/1033/content.aspx>>.
- ⁴⁹ [Http://mmrc.caltech.edu](http://mmrc.caltech.edu) [online]. 2001 [cit. 2011-05-10]. [Http--mmrc.caltech.edu-FTIR-FTIRintro.pdf](http://mmrc.caltech.edu-FTIR-FTIRintro.pdf). Dostupné z WWW: <<http://mmrc.caltech.edu/FTIR/FTIRintro.pdf>>.
- ⁵⁰ SWAPP, Susan. [Http://serc.carleton.edu/index.html](http://serc.carleton.edu/index.html) [online]. University of Wyoming : April 02, 2011 [cit. 2011-04-24]. Scanning Electron Microscopy (SEM). Dostupné z WWW: <http://serc.carleton.edu/research_education/geochemsheets/techniques/SEM.html>.
- ⁵¹ [Http://mse.iastate.edu](http://mse.iastate.edu) [online]. Iowa State University : 2006 [cit. 2011-04-24]. Electron Source. Dostupné z WWW: <<http://mse.iastate.edu/microscopy/home.html>>.

7 LIST OF ABBREVIATIONS

HP	Heterogeneous Photocatalysis
SC	Semiconductor
VB	Valence band
CB	Conduction band
SDR	Structural Directing Reagent
CS	Continual stream
DOD	Drop-on-Demand
DCIP	2,6-dichloroindophenol
TTIP	Titanium(IV)isopropoxide
CA	Contact angle
FT-IR	Fourier Transform InfraRed spectrometry
SEM	Scanning electron microscopy